Cold Flow Modeling of a Two-Stroke Engine

Faruk YILDIZ

Ahmet TUNA

Department of Mechanical Engineering

Engineering Faculty

Marmara University

Istanbul/Turkey

February 2014

Supervisor: Assist. Prof. Dr. Mustafa YILMAZ

Approval of the thesis:

Cold Flow Modeling of a Two-Stroke Engine

submitted by **FARUK YILDIZ** and **AHMET TUNA** in partial fulfillment of the requirements for undergraduate academic degree in Mechanical Engineering Department, Marmara University by,

Prof. Dr. Ertuğrul TAÇGIN _____
Dean of the Engineering Faculty, Marmara University

Prof. Dr. A. Kerim KAR _____
Chairman of Mechanical Engineering Dept., Marmara University

Assist. Prof. Dr. Mustafa YILMAZ _____
Superviser, Mechanical Engineering Dept., Marmara University

Date: …../..…/…….

ACKNOWLEDGEMENTS

While doing this research, we have been helped by so many people. They have contributed towards our understanding, knowledge, and also guidance to improve our skills. In general, we express our sincere appreciation this main thesis to our supervisor, Assist. Prof. Dr. Mustafa YILMAZ for his helpful supervision, advice and continuous encouragement that really helps, positive criticism and suggestion throughout this project. Having him around gives this project worked done. Also, special thankful to Prelector Hasan KÖTEN for sharing his expertise in CFD simulation.

Our thankful also our parents. Without their support, this thesis would never be here. Moreover, we would like to thanks for all our friends who has provides assistance at every aspect during this project. Their view tips are useful indeed in helping us to achieve doing this thesis.

Abstract

The aim of this study is to see the conditions inside the cylinder by modeling the in-cylinder air flow. The project is based on two stroke engine and CFD. The objective of this project is to model two stroke engine using a 3-Dimensional software (Commercial CFD Solver). Fluid geometry in cylinder is designed and this geometry is meshed. Then, initial conditions are indicated and model is solved at 4000 rpm. The 3-Dimensional software that using as a part of this work solves the thermodynamic and Navier Stoke equations numerically on the backside.

Keywords: Two-stroke engine, CFD, 3-Dimensional modeling

Table of Contents

1 Introduction

Cold flow modeling of a two stroke engine was made with using a Commercial CFD Solver in this study. This model gives us the chance of controlling air motion in cylinder. Optimizations owing to this project can be made. If a well design cold flow in cylinder is created, more efficient combustion cycle can be achieved. This gives us, less fuel consumption, more power, less emissions. This project is intended to achieve a clean world.

In this area, there are many researches. Great parts of these researches are about low emissions. In 2002 the European Commission adopted a European Union strategy to reduce atmospheric emissions from seagoing ships. The strategy reports on the magnitude and impact of ship emissions in the EU, and sets out a number of actions to reduce the contribution of shipping to health and climate change. One possible approach for the reduction of NO_x and soot emissions of marine diesel engines is the use of multiple injection strategies, similar to the ones used in automotive diesel engines. In this way, diesel combustion could be optimized with respect to pollutant emissions, without compromising fuel efficiency. Panagiotis Kontoulis, Christos Chryssakis and Lambros Kaiktsis have worked about on this subject to decrease the emissions. They have used KIVA-3 code as the modeling platform [1]. In recent years, the request for low exhaust emissions and high thermal efficiency has become stringent in many countries for the purpose of environmental protection. In the state of California, USA, Tier 2 emission regulation went into effect in 2000. So Yoshio Kobayashi, Yukiteru Yoshida, Kazuyuki Uenoyama, Kazunori Kudo and Hiroyuki Endo have investigated low exhaust emission system for small two-stroke cycle engines. For this reason, they have improved the new scavenging technology and the development of 5 new TLE series engine models [2]. S. Scott Goldsborough and Peter Van Blarigan have investigated high efficiency and low emissions on a free piston engine. A free piston internal combustion (IC) engine operating on high compression ratio (CR) homogeneous charge compression ignition (HCCI) combustion is being developed by Sandia National Laboratories to significantly improve the thermal efficiency and exhaust emissions relative to conventional crankshaft-driven SI and Diesel engines. A two-stroke scavenging process recharges the engine and is key to realizing the efficiency and emissions potential of the device. To ensure that the engine's performance goals can be achieved the scavenging system was configured using computational fluid dynamics (CFD), zero- and one dimensional modeling, and single step parametric variations. A wide range of design options was investigated including the use of loop, hybrid-loop and uniflow scavenging methods, different charge delivery options, and various operating schemes. Parameters such as the intake/exhaust port arrangement, valve lift/timing, charging pressure and piston frequency were varied. Operating schemes including a standard uniflow configuration, a low charging pressure option, a stratified scavenging geometry, and an over-expanded (Atkinson) cycle were studied. The computational results indicated that a stratified scavenging scheme employing a uniflow geometry, and supplied by a stable, low temperature/pressure charge will best optimize the efficiency and emissions characteristics of the engine. The operating CR can be maximized through substantial replacement of the burned charge, while short-circuiting emissions can be controlled by late fuel introduction.

The in-cylinder flows are important to both NO_x and short-circuiting emissions with inadequate mixing (and resulting temperature stratification) the predominant driver of NO production, and fuel penetration to the exhaust valve region the main cause of unburned hydrocarbon emissions [3].

J.Galindo, H. Climent, B. Plá, V. D. Jiménez have worked about correlations for Wiebe function parameters for combustion simulation in two stroke small engines [4]. When the history of development of CFD analysis is looked, the effect of mathematical models can be clearly seen. The time process for this process of filling and emptying of cylinder contents gets shorter and shorter as the engine speed increases [5]. Mathematical description of this dynamic process has not been easy and many experimental and mathematical tools have been used in the past to understand this dynamic phenomenon. Jante was the first to develop a useful tool with the combustion of pitot tubes to study and evaluate the scavenging process inside the cylinder of a 2-stroke engine [6]. Many attempts have been made after the experiments of Jante. Sher has reported practical methods to study the scavenging process [7]. Reddy et al. have studied the in-cylinder air movement in a 2-stroke engine hot wire anemometer [8]. Ikeda et al. have conducted scavenging flow measurements in a 2-stroke engine by Fiber Laser Doppler Velocimeter (FLDV) on a Suzuki 100 cc engine for motored and fired conditions [9]. Hilbert and Falco have develop a new measurement technique using Laser Induced Photochemical Anemometry for evaluating velocity and velocity gradients over a chosen plane in a motored 2-stroke engine during scavenging [10]. A part from the above, many attempts, as chronicled by Heywood and Sher have been made to study in-cylinder parameters in an IC engine employing mathematical tools [11]. Amsden et al. have developed a comprehensive model for 2D and 3D engine simulations using a KIVA code followed [12], by Changyou and Wallace [13], Raghunathan and Kenny [14], Epstein et al. [15] and Yang et al. [16], have proposed the Reynolds Stress Turbulence Model (RSTM) for anisotropic turbulence engine flows and have modified the KIVA code to include RSTM for simulation of combustion and direct injection. Basha and Gopal have investigated the research undertaken between 1978 and 2008 in respect of in-cylinder fluid flow, turbulence and spray characteristics and have concluded that some scientists considered the Re-Normalized Group (RNG) k-ε model as the best suited for engine simulations [17]. Verhelst and Sheppard [18], have proposed a unified approach to sub-models involved in multi-zone modeling of engine simulation especially for turbulent combustion modeling [19].Mathematical models are generally used for modeling in engineering. Especially, the Computational Fluid Dynamics is based on mathematical models. There are lots of names who worked to find these models. Years and years later, now, their models on CFD analysis are used by the researchers and us. J.Galindo, H. Climent, B. Plá, V. D. Jiménez used Wiebe Function for combustion analysis. They took 2 engines for their experiment. One of them is 50cc, the other one is 125cc. They have found out Wiebe parameters using experimental data of two engines, to simulate these two engines. Then, they compared simulation data with the each other, to be 50cc and 125cc [4]. R. Mikalsen and A. P. Roskilly have investigated the in-cylinder gas motion, combustion process and nitrogen oxide formation in a free-piston diesel engine and compare the results to those of a conventional engine, using a computational fluid dynamics engine model [20].

On the other hand, micro scale engines are very useful for small machines but how much their limits can be minimized. Considerable effort has been devoted in recent years to building miniature heat engines as battery replacements and prime-movers for micro-air vehicle propulsion. Simple thermodynamic analysis Show that as a heat engine is miniaturized, it becomes less thermodynamically efficient. A critical length scale exists at which losses outstrip power production and cycle efficiency goes to zero. The objectives of these researches are to identify a minimum practical length scale for two stroke piston engines and investigate the processes responsible for setting this limit. The performance of 7 engines weighing 15g to 500g is studied using a specially designed dynamometer. Peak power outputs have been measured at 8-278W with peak efficiencies ranging from 3-9%. A scaling analysis similar to one established for conventional scale engines shows the minimum displacement for a 'practical' IC engine to be between 0.5 and 1 cc [21].

Combustion analysis has been conducted on a small two stroke glow ignition engine, which has similar combustion characteristics to homogeneous charge compression ignition (HCCI) engines. Difficulties such as unknown ignition timing and the polytrophic index have been addressed by combining both heat release and mass fraction burn analysis. Results for all operating condition have shown good correlations between the two methods. Traditionally, burn rate analysis is widely used for spark ignition engines, while the heat release analysis is more suitable for compression ignition engines. Miniature engines do not fall into either category. In spark ignition engines, the mixture is premixed and the combustion is initiated by a spark, so the time of the start of combustion is known. In compression engines, combustion starts from autoignition of the fuel. The start of combustion is unknown but it has to be later than the fuel injection timing. This miniature engine, with a premixed mixture and glow plug assisted auto ignition is special case. It is likely that the compression and ignition processes would be most similar to homogeneous charge compression ignition (HCCI) engines [22].

2 Two stroke engine

A two-stroke, two-cycle, or two-cycle engine is a type of internal combustion engine which completes a power cycle in only one crankshaft revolution and with two strokes, or up and down movements, of the piston in comparison to a "four-stroke engine", which uses four strokes to do so. This is accomplished by the end of the combustion stroke and the beginning of the compression stroke happening simultaneously and performing the intake and exhaust (or scavenging) functions at the same time.

Two-stroke engines often provide high power-to-weight ratio, usually in a narrow range of rotational speeds called the "power band", and, compared to 4-stroke engines, have a greatly reduced number of moving parts, are more compact and significantly lighter.

Gasoline (spark ignition) versions are particularly useful in lightweight (portable) applications such as chainsaws and small, lightweight and racing motorcycles, and the concept is also used in diesel compression ignition engines in large and weight insensitive applications, such as ships, locomotives and electricity generation. The heat transfer from the engine to the cooling system is less in a two-stroke engine than in a traditional four-stroke, a fact that adds to the

overall engine efficiency; however, traditional 2-strokes have a poor exhaust emissions feature [23].

2.1 History of two stroke engine

It is generally accepted that the two-stroke cycle engine was invented by Sir Dugald Clerk in England at the end of the 19th Century. The form of the engine using crankcase compression for the induction process, including the control of the timing and area of the exhaust, transfer and intake ports by the piston, was patented by Joseph Day in England in 1891. His engine was the original "three-port" engine and is the forerunner of the simple two-stroke engine which has been in common usage since that time.

Some of the early applications were produced in motorcycle form and are well recorded by Caunter. The first engines were produced by Edward Butler in 1887 and by J. D. Roots, in the form of the Day crankcase compression type, in 1892; both of these designs were for powered tricycles. Considerable experimentation and development was conducted by Alfred Scott, and his Flying Squirrel machines competed very successfully in Tourist Trophy races in the first quarter of the 20th Century. They were designed quite beautifully in both the engineering and in the aesthetic sense. After that, two-stroke engines faded somewhat as competitive units in racing for some years until the supercharged DKW machines of the '30s temporarily revived their fortunes. With the banning of supercharging for motorcycle racing after the Second World War, the two-stroke engine lapsed again until 1959 when the MZ machines, with their tuned exhaust expansion chambers and disc valve induction systems, introduced a winning engine design which has basically lasted to the present day. Today, two-stroke-engine motorcycles, scooters and mopeds are still produced in very large numbers for general transport and for recreational purposes, although the legislative pressure on exhaust emissions in some countries has produced a swing to a four-stroke engine replacement in some cases. Whether the two-stroke engine will return as a mass production motorcycle engine will depend on the result of research and development being conducted by all of the manufacturers at the present time. There are some other applications with engines which are very similar in design terms to those used for motorcycles, and the sports of go-kart and hydroplane racing would fall into this category.

The two-stroke engine is used for lightweight power units which can be employed in various attitudes a handheld power tools. Such tools are chainsaws, brush cutters and concrete saws, to name but a few, and these are manufactured with a view to lightness and high specific power performance. The manufacturing numbers involved are in millions per annum worldwide.

The earliest outboard motors were pioneered by Evinrude in the United States about 1909, with a 1.5 hp unit, and two-stroke engines have dominated this application until the present day. Some of the current machines are very sophisticated designs, such as 300 hp V6 and V8-engined outboards with remarkably efficient engines considering that the basic simplicity of the two-stroke crankcase compression engine has been retained. Although the image of the outboard motor is that it is for sporting and recreational purposes, the facts are that the

product is used just as heavily for serious employment in commercial fishing and for everyday water transport in many parts of the world.

Some of the new recreational products which have appeared in recent times are snowmobiles and water scooters, and the engine type almost always employed for such machines is the two-stroke engine. The use of this engine in a snowmobile is almost an ideal application, as the simple lubrication system of a two-stroke engine is perfectly suited for sub-zero temperature conditions. Although the snowmobile has been described as a recreational vehicle, it is actually a very practical means of everyday transport for many people in an Arctic environment.

The use of the two-stroke engine in automobiles has had an interesting history, and some quite sophisticated machines were produced in the 1960s, such as the Auto-Union vehicle form West Germany and the simpler Wartburg from East Germany. The Saab car from Sweden actually won the Monte Carlo Rally with Eric Carlson driving it. Until recent times, Suzuki built a small two-stroke-engined car in Japan. With increasing ecological emphasis on fuel consumption rate and exhaust emissions, the simple two-stroke-engined car disappeared, but interest in the design has seen a resurgence in recent times as the legislative pressure intensifies on exhaust acid emissions. Almost all car manufacturers are experimenting with various forms of two-stroke-engined vehicles equipped with direct fuel injection, or some variation of that concept in term of stratified charging or combustion.

The two-stroke engine has been used in light aircraft, and today is most frequently employed in the recreational microlite machines. There are numerous other applications for the spark-ignition (SI) engine, such as small electricity generating sets or engines for remotely piloted vehicles, i.e., aircraft for meteorological data gathering or military purposes. These are but two of a long list of multifarious examples.

The use of the two-stroke engine in compression ignition (CI) or diesel form deserves special mention. The engine type has been used for trucks and locomotives, such as the design from General Motors in America or Rootes-Tilling-Stevens in Britain. Both of these have been very successful engines in mass production. The engine type, producing a high specific power output, has also been a favorite for military installations in tanks and fast naval patrol boats. Some of the most remarkable aircraft engines ever built have been two-stroke diesel units, such as the Junkers Jumo and the turbo-compounded Napier Nomad. There is no doubt that the most successful of all of the applications is that of the marine diesel main propulsion unit. The complete engine is usually some 12 m. tall, so the description is rather apt. Such engines, the principal exponents of which were Burmeister and Wain in Copenhagen and Sulzer in Winterthur, were typically of 900 mm. bore and 1800 mm. stroke and ran at 60-100 rpm, producing some 400 hp per cylinder. They had thermal efficiencies in excess of 50%, making them most efficient prime movers ever made. These engines are very different from the rest of the two-stroke engine species in terms of scale but not in design concepts.

The diesel engine, like its spark-ignition counterpart, is also under legislative pressure to conform to ever-tighter emissions standards. For the diesel engine, even though it provides very low emissions of carbon monoxide and of hydrocarbons, does emit visible smoke in the

form of carbon particulates and measurable levels of nitrogen oxides. The level of emission of both of these latter components is under increasing environmental scrutiny and the diesel engine must conform to more stringent legislative standards by the year 2000. The combination of very low particulate and NO_x emission is a tough R&D proposition for the designer of some 50% at its richest setting to avoid excessive exhaust smoke, the exhaust gas is oxygen rich and so only a lean burn catalyst can be used on either a two-stroke or a four-stroke cycle engine. This does little, if anything at all, to reduce the nitrogen oxide emissions. Thus the manufacturers are again turning to the two-stroke cycle diesel engine as a potential alternative powerplant for cars and trucks, as that cycle has inherently a significantly lower NO_x emission characteristic. Much R&D is taking place in the last decade of the 20^{th} Century with a view to eventual manufacture, if the engine meets all relevant criteria on emissions, thermal efficiency and durability.

It is probably true to say that the two-stroke engine has produced the most diverse opinions on the part of both the users and the engineers. These opinions vary from fanatical enthusiasm to thinly veiled dislike. The engine seems so deceptively simple to design, develop and manufacture. That the very opposite is the case may well be the reason that some spend a lifetime investigating this engineering curiosity. The potential rewards are great, for no other engine cycle has produced, in one constructional form or another, such high thermal efficiency or such low specific fuel consumption, such high specific power criteria referred to either swept volume, bulk or weight, nor such low acid exhaust emissions [24].

2.2 The fundamental method of operation a simple two-stroke engine

The simple two-stroke engine is shown in Fig. 2.1, with the various phases of the filling and emptying of the cylinder illustrated in (a)-(d). The simplicity of the engine is obvious with all of the processes controlled by the upper and lower edges of the piston.

In Fig. 1.1(a), above the piston, the trapped air and fuel charge is being ignited by the spark plug, producing a rapid rise in pressure and temperature which will drive the piston down on the power stroke. Below the piston, the opened inlet port is including air from the atmosphere into the crankcase due to the increasing volume of the crankcase lowering the pressure below the atmospheric value. The crankcase is sealed around the crankshaft to ensure the maximum depression within it. To induce fuel into the engine, the various options exits of either placing a carburetor in the inlet tract, injecting fuel directly into the cylinder before or after the closure of the exhaust port. Clearly, if it is desired to operate the engine as a diesel power unit, the latter is the only option, with the spark plug possibly being replaced by a glow plug as an initial starting aid and the fuel injector placed in the cylinder head area.

In Fig. 2.1(b), above the piston, the exhaust port has been opened. It is often called the "release" point in the cycle, and this allows the transmission into the exhaust duct of a pulse of hot, high-pressure exhaust gas from the combustion process. As the area of the port is increasing with crankshaft angle, and the cylinder pressure is falling with time, it is clear that the exhaust duct pressure profile with time is one which increases to a maximum value and then decays. Such a flow process is described as unsteady gas flow and such a pulse can be reflected from all pipe area changes, or at the pipe end termination to the atmosphere. These

reflections have a dramatic influence on the engine performance. Below the piston, the compression of the fresh charge is taking place. The pressure and temperature achieved will be a function of the proportionate reduction of the crankcase volume, i.e., crankcase compression ratio.

In Fig. 2.1(c), above the piston, the initial exhaust process, referred to as "blowdown", is nearing completion and, with the piston having uncovered the transfer ports, this connects the cylinder directly to the crankcase through the transfer ducts. If the crankcase pressure exceeds the cylinder pressure then the fresh charge enters the cylinder in what is known as the scavenge process. Clearly, if the transfer ports are badly directed then the fresh charge can exit directly out of the exhaust port and be totally lost from the cylinder. Such a process, referred to as "short-circuiting", would result in the cylinder being filled only with exhaust gas at the onset of the next combustion process, and no pressure rise or power output would a consequential monstrous emission rate of unburned hydrocarbons. Therefore, the directioning of the fresh charge by the orientation of the transfer ports should be conducted in such a engine, for the highest trapped air mass can be burned with an appropriate fuel quantity to attain the optimum power output. It is obvious that the scavenge process is one which needs to be optimized to the best of the designer's ability. Equally, no scavenge process, however extensive or thorough, will ever leach out last molecule of exhaust gas.

In Fig. 2.1(d), in the cylinder, the piston is approaching what is known as the "trapping" point, or exhaust closure. The scavenge process has been completed and the cylinder is now filled with a mix of air, fuel if a carbureted design, and exhaust gas. As the piston rises, the cylinder pressure should also rise, but the exhaust port is still open and, barring the intervention of some unsteady gas-dynamic effect generated in the exhaust pipe, the piston will spill fresh charge into the exhaust duct to the detriment of the resulting power output and fuel consumption. Should it be feasible to gas-dynamically plug the exhaust port during this trapping phase, then it is possible to greatly increase the performance characteristic of the engine. In a single-cylinder racing engine, it is possible to double the mass of the trapped air charge using a tuned pipe, which means doubling the power output. After the exhaust port is finally closed, the true compression process begins until the combustion process is commenced by ignition. Not surprisingly, therefore, the compression ratio of a two-stroke engine is characterized by the cylinder volume after exhaust port closure and is called the trapped compression ratio to distinguish it from the value commonly quoted for the four-stroke engine. That value is termed here as the geometric compression ratio and is based on the full swept volume.

In summary, the simple two-stroke engine is a double-acting device. Above the piston, the combustion and power processes take the place, whereas below the piston in the crankcase, the fresh charge is induced and prepared for transfer to the upper cylinder [25].

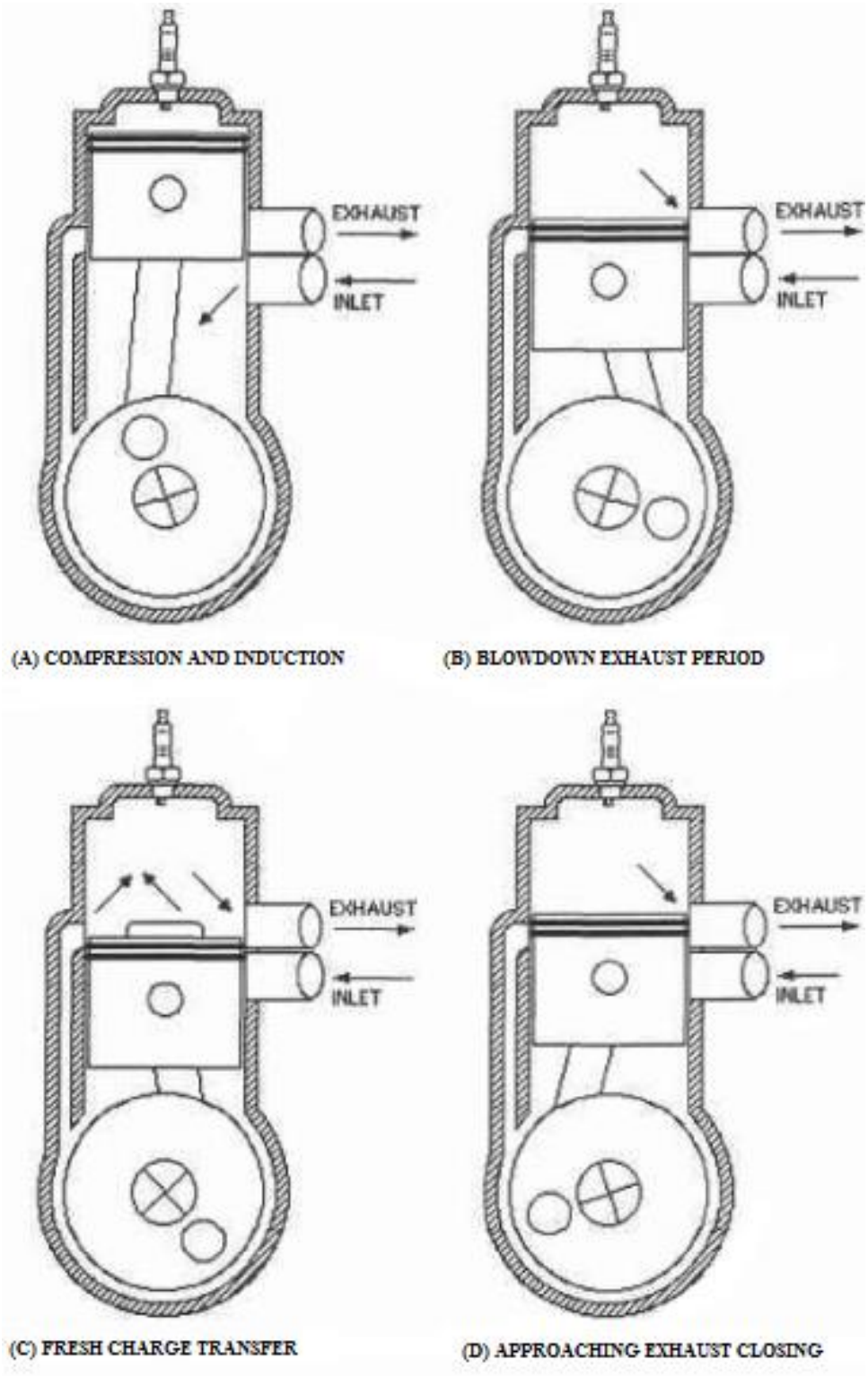

Fig. 2.1 Various stages in the operation of the two-stroke cycle engine [26]

3 Thermodynamics terms

3.1 Scavenge ratio and delivery ratio

In Fig. 1.1(c), the cylinder has just experienced a scavenge process in which a mass of fresh charge, m_{as}, has been supplied through the crankcase from the atmosphere. By measuring the atmospheric, i.e. the ambient pressure and temperature, P_{at} and T_{at}, the air density will be given by ρ_{at} from the thermodynamic equation of state, where R_a is the gas constant for air:

$$\rho_{at} = \frac{P_{at}}{R_a T_{at}} \quad \text{(Eq. 3.1)}$$

The delivery ratio, DR, of the engine defines the mass of air supplied during the scavenge period as a function of a reference mass, m_{dref}, which is that mass required to fill the swept volume under the prevailing atmospheric conditions, i.e.:

$$m_{dref} = \rho_{at} V_{sv} \quad \text{(Eq. 3.2)}$$

$$DR = \frac{m_{as}}{m_{dref}} \quad \text{(Eq. 3.3)}$$

The scavenge ratio, SR, of a naturally aspirated engine defines the mass of air supplied during the scavenge period as a function of a reference mass, m_{sref}, which is the mass that could fill the entire cylinder volume under the prevailing atmospheric conditions, i.e.:

$$m_{sref} = \rho_{at}(V_{sv} + V_{cv}) \quad \text{(Eq. 3.4)}$$

$$SR = \frac{m_{as}}{m_{sref}} \quad \text{(Eq. 3.5)}$$

The SAE Standard J604d refers to and defines delivery ratio. For two-stroke engines the more common nomenclature in the literature is “scavenge ratio”, but is should be remembered that the definitions of these air-flow ratios are mathematically different.

Should the engine be supercharged or turbocharged, then the new reference mass, m_{sref}, for the estimation of scavenge ratio is calculated from the state conditions of pressure and temperature of the scavenge air supply, P_s and T_s.

$$\rho_s = \frac{P_s}{R_a T_s} \quad \text{(Eq. 3.6)}$$

$$SR = \frac{m_{as}}{\rho_s (V_{sv}+V_{cv})} \quad \text{(Eq. 3.7)}$$

The above theory has been discussed in terms of the air flow referred to the swept volume of a cylinder as if the engine is a single-cylinder unit. However, if the engine is a multi-cylinder device, it is the total swept volume of the engine that is under consideration [27].

3.2 Scavenging efficiency and purity

The scavenging efficiency is defined as the mass of delivered air that has been trapped, m_{tas}, by comparison with the total mass of charge, m_{tr}, that is retained at exhaust closure. The

trapped charge is composed only of fresh charge trapped, m_{tas}, and exhaust gas, m_{ex}, and any air remaining unburned from the previous cycle, m_{ar}, where:

$$m_{tr} = m_{tas} + m_{ex} + m_{ar} \quad \text{(Eq. 3.8)}$$

Hence, scavenging efficiency, SE, defines the effectiveness of the scavenging process, as can be from the following statement:

$$SE = \frac{m_{tas}}{m_{tr}} = \frac{m_{tas}}{m_{tas}+m_{ex}+m_{ar}} \quad \text{(Eq. 3.9)}$$

However, the ensuing combustion process will take place between all of the air in the cylinder with all of the fuel supplied to that cylinder, and it is important to define the purity of the trapped charge in its entirety. The purity of the trapped charge, Π, is defined as the ratio of air trapped in the cylinder before combustion, m_{ta}, to the total mass of cylinder charge, where: [28]

$$m_{ta} = m_{tas} + m_{ar} \quad \text{(Eq. 3.10)}$$

$$\Pi = \frac{m_{ta}}{m_{tr}} \quad \text{(Eq. 3.11)}$$

In many technical papers and textbooks on two-stroke engines, the words "scavenging efficiency" and "purity" are somewhat carelessly interchanged by the authors, assuming prior knowledge by the readers. They assume that the value of m_{ar} is zero, which is generally true stoichiometric, but it would not be true for two-stroke diesel engines where the air is never totally consumed in the combustion process, and it would not be true for similar reasons for a stratified combustion process in a gasoline-fueled spark-ignition engine.

3.3 Trapping efficiency

Trapping efficiency, TE, is the capture ratio of mass of delivered air that has been trapped, m_{tas}, to that supplied, m_{as}, or:

$$TE = \frac{m_{tas}}{m_{as}} \quad \text{(Eq. 3.12)}$$

It will be seen that expansion of Eq. 3.12 gives:

$$TE = \frac{m_{tr}\, SE}{m_{sref}\, SR} \quad \text{(Eq. 3.13)}$$

It will also be seen under ideal conditions, that m_{tr} can be considered to be equal to m_{sref} and that Eq. 3.13 can be simplified in an interesting manner, i.e. [28],

$$TE = \frac{SE}{SR}$$

3.4 Charging efficiency

Charging efficiency, CE, expresses the ratio of the filling of the cylinder with air, by comparison with filling that same cylinder perfectly with air at the onset of the compression stroke. After all, the object of the design exercise is to fill the cylinder with the maximum

quantity of air in order to burn a maximum quantity of fuel with that same air. Hence, charging efficiency, CE, is given by:

$$CE = \frac{m_{tas}}{m_{sref}} \quad \text{(Eq. 3.14)}$$

It is also the product of trapping efficiency and scavenge ratio, as shown here:

$$CE = \frac{m_{tas}}{m_{as}} \times \frac{m_{as}}{m_{sref}} = TE \times SR \quad \text{(Eq. 3.15)}$$

It should be made quite clear that this definition is not precisely as defined in SAE J604d. in that SAE nomenclature Standard, the reference mess is declared to be m_{dref} from Eq. 3.2, and not m_{sref} as used from Eq. 3.4. My defense for this is " custom and practice in two-stroke engines", the fact that it is all of the cylinder space that is being filled and not just the swept volume, the convenience of charging efficiency assessment by the relatively straight-forward experimental acquisition of trapping efficiency and scavenge ratio [29].

3.5 Air-to-fuel ratio

It is important to realize that there are narrow limits of acceptability for the combustion of air and fuel, such as gasoline or diesel. In the case of gasoline, the ideal fuel is octane, C_8H_{18}, which burns "perfectly" with air in a balanced equation called the stoichiometric equation. Most students will recall that air is composed, volumetrically and molecularly, of 21 parts oxygen and 79 parts nitrogen. Hence, the chemical equation for complete combustion becomes:

$$2C_8H_{18} + 25[O_2 + \frac{79}{21} N_2] = 16\ CO_2 + 18\ H_2O + 25\frac{79}{21} N_2 \quad \text{(Eq. 3.16)}$$

This produces the information that the ideal stoichiometric air-to-fuel ratio, AFR, is such that for every two molecules of octane, 25 molecules of air are needed. As the information in mass terms are normally needed , then as the molecular weights of O_2, H_2, N_2 are simplistically 32, 2 and 28, respectively, and the atomic weight of carbon C is 12, then:

$$\text{AFR} = \frac{25 \times 32 + 25 \times 28 \times \frac{79}{28}}{2\ (8 \times 12 + 18 \times 1)} \quad \text{(Eq. 3.17)}$$

As the equation is balanced, with the exact amount of oxygen being supplied to burn all of the carbon to carbon dioxide and all of the hydrogen to steam, such a burning process yields the minimum values of carbon monoxide emission, CO, and unburned hydrocarbons, HC. Mathematically speaking they are zero, and in practice they are also at a minimum level. As this equation would also produce the maximum temperature at the conclusion of combustion, this gives the highest value of emissions of NO_x, the various oxides of nitrogen. Nitrogen and oxygen combine at high temperatures to give such gases as N_2O, NO, etc [30].

3.6 Cylinder trapping ratio

The point of the foregoing discussion is to make you aware that the net effects of the cylinder scavenge process is to fill the cylinder with of air, m_{ta}, within a total mass of charge, m_{tr}, at

the trapping point. This total mass is highly dependent on the trapping pressure, as the equation of state shows:

$$m_{tr} = \frac{P_{tr}\, V_{tr}}{R_{tr}\, T_{tr}} \quad \text{(Eq. 3.18)}$$

where

$$V_{tr} = V_{ts} + V_{cv} \quad \text{(Eq. 3.19)}$$

In any given case, the trapping volume, V_{tr}, is a constant. This is also true of the gas constant, R_{tr}, for gas at the prevailing gas composition at the trapping point. The gas constant for exhaust gas, R_{ex}, is almost identical to the value for air, R_a. Because the cylinder gas composition is usually mostly air, the treatment of R_{tr} as being equal to R_a invokes little error. For any one trapping process, over a wide variety of scavenging behavior, the value of trapping temperature, T_{tr}, would rarely change by 5%. Therefore, it is the value of trapping pressure, P_{tr}, that is the significant variable. As stated earlier, the value of trapping pressure is directly controlled by the pressure wave dynamics of the exhaust system, be it a single-cylinder engine with or without a tuned exhaust system, or a multi-cylinder power unit with a branched exhaust manifold [31]. The value of the trapped fuel quantity, m_{tf}, can be determined from:

$$m_{tf} = \frac{m_{ta}}{AFR_t} \quad \text{(Eq. 3.20)}$$

3.7 Heat released during the burning process

The total value of the heat that will be released from the combustion of this quantity of fuel will be Q_R:

$$Q_R = \eta_c\, m_{tf}\, C_{fl} \quad \text{(Eq. 3.21)}$$

where η_c is the combustion efficiency and C_{fl} is the (lower) calorific value of the fuel [32].

3.8 The thermodynamic cycle for the two-stroke engine

This is often referred to as a derivative Otto Cycle. The result of the calculation of a theoretical cycle can be observed in Figs. 3.1 and 3.2, by comparison with measured pressure-volume data from an engine of the same compression ratios, both trapped and geometric. In the measured case, the cylinder pressure data are taken from a 400 cm^3 single-cylinder two-stroke engine running at 3000 rpm at wide open throttle. In the theoretical case, and this is clearly visible on the log p-log V plot in Fig. 3.2, the following assumptions are made: (a) compression begins at trapping, (b) all heat release (combustion) takes place at TDC at constant volume, (c) the exhaust process is considered as a heat rejection process at release, (d) the compression and expansion processes occur under ideal, or isentropic, conditions within air as the working fluid, and so those processes are calculated as:

$$P\, V^{\gamma} = constant$$

where γ is a constant. For air, the ratio of specific heats, γ, has a value of 1.4. A fundamental theoretical analysis would show that the thermal efficiency, η_t, of the cycle is given by:

$$\eta_t = 1 - \frac{1}{C\, R_t^{\gamma-1}} \qquad \text{(Eq. 3.22)}$$

Thermal efficiency is defined as:

$$\eta_t = \frac{work\ produced\ per\ cycle}{heat\ available\ as\ input\ per\ cycle} \qquad \text{(Eq. 3.23)}$$

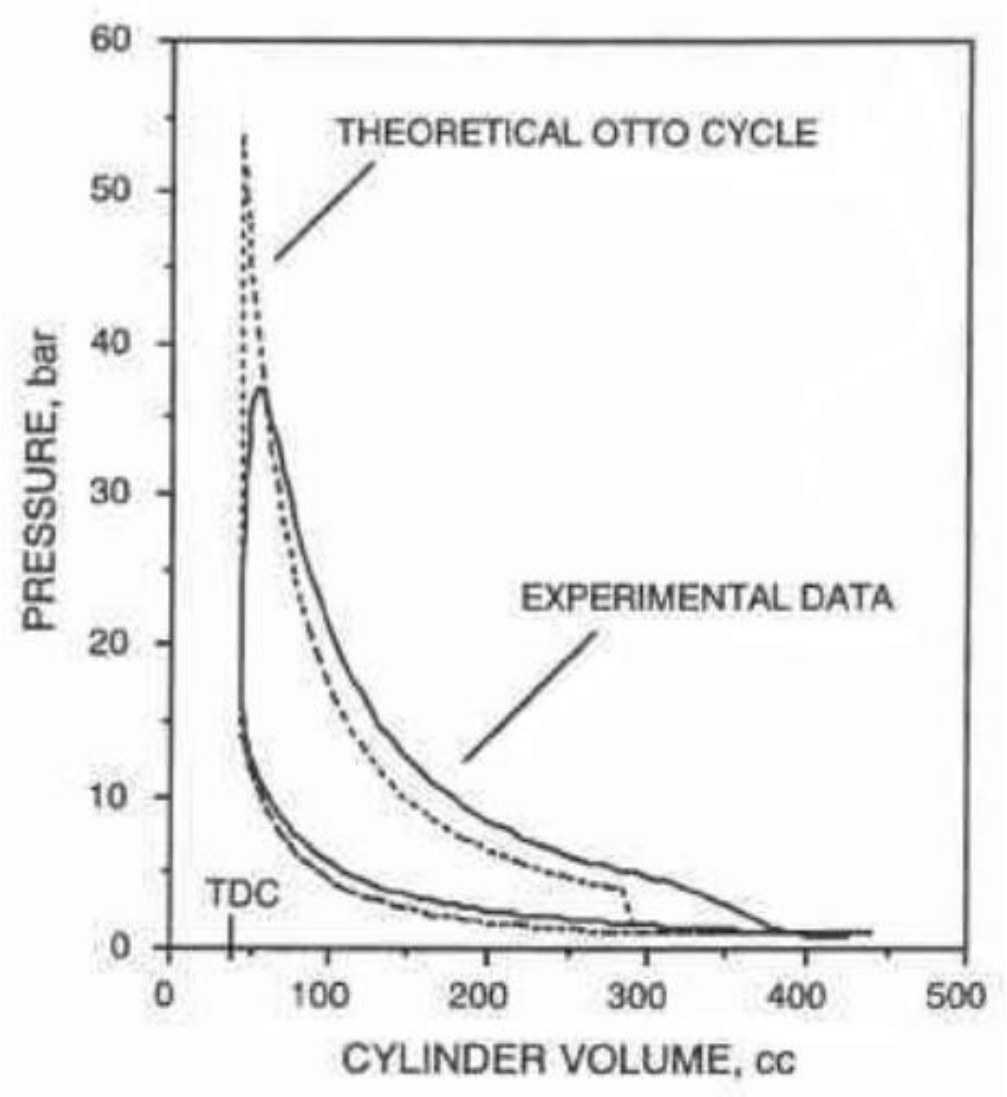

Fig. 3.1 Otto cycle comparison with experimental data [11]

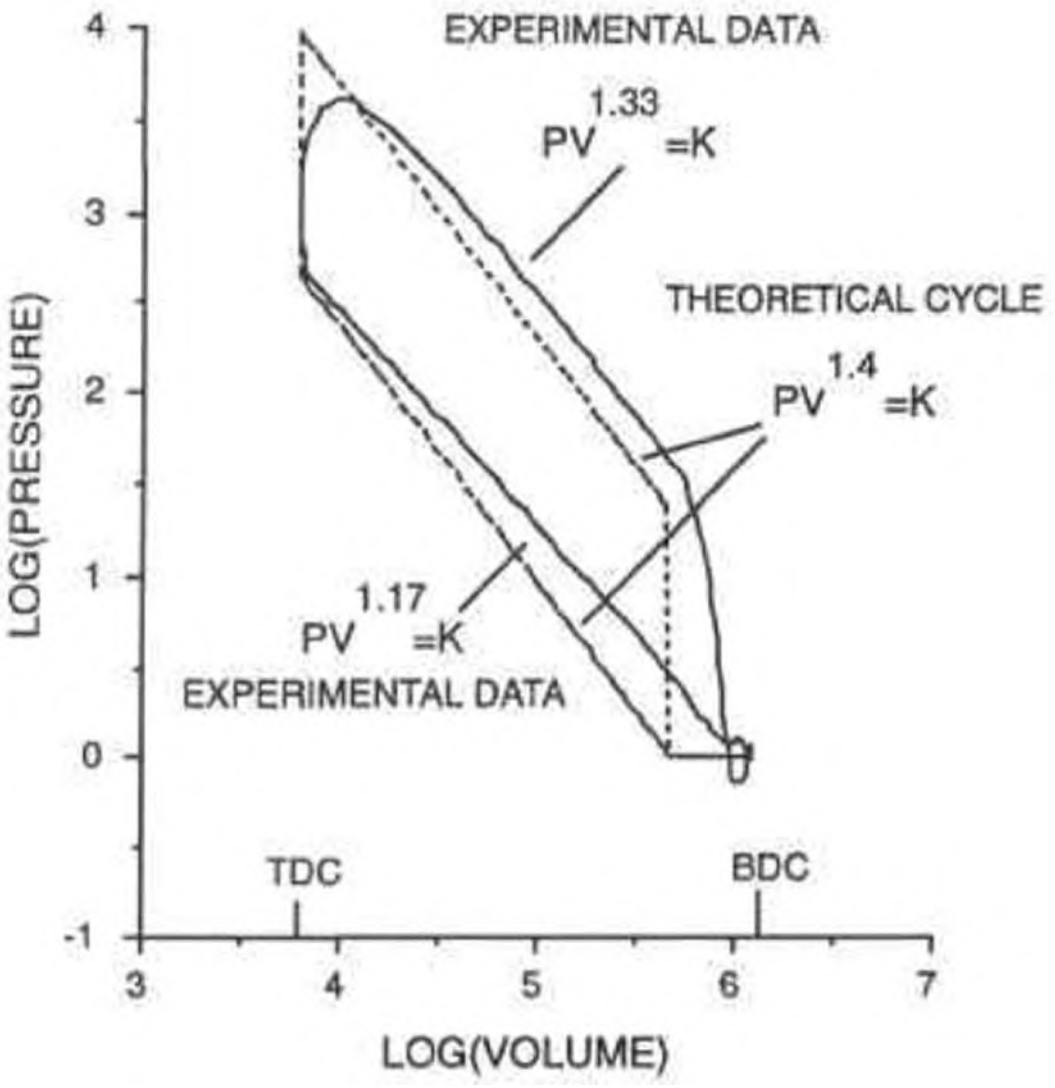

Fig 3.2 Logarithmic plot of pressure and volume [33]

The work on the piston during the cycle is ultimately and ideally and ideally the work delivered to the crankshaft by the connecting rod. The word "ideal" in thermodynamic terms means that the friction or other losses, like leakage past the piston, are not taken into consideration in the statement made above. Therefore, the ideal work produced per cycle is that work carried out on the piston by the force, F, created from the gas pressure, p. Work is always the product of force and distance, x, moved by that force, so, where A is the piston area:

$$Work\ produced\ per\ cycle = \int Fdx = \int PAdx = \int PdV \qquad \text{(Eq. 3.24)}$$

Therefore, the work produced for any given engine cycle, in the case of a two-stroke engine for one crankshaft revolution from TDC to TDC, is the cyclic integral of the pressure-volume diagram in the cylinder above the piston. By the same logic, the pumping work required in the crankcase is the cyclic integral of the pressure-volume diagram, be it a theoretical cycle or the actual cycle as illustrated in Fig. 3.1 [33]. The above statements are illustrated in Fig. 3.3 for the actual data shown previously in Figs. 3.1 and 3.2.

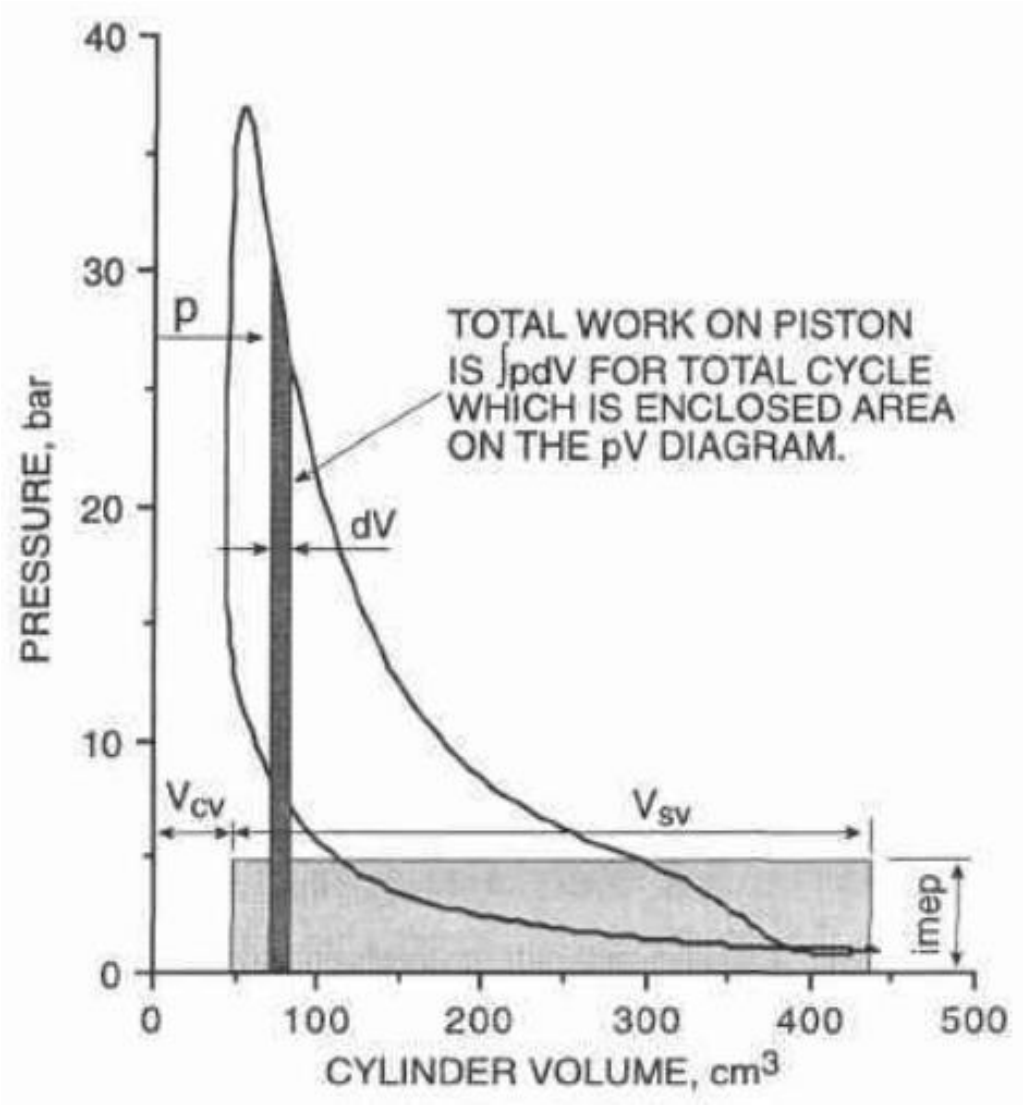

Fig. 3.3 Determination of imep from the cylinder P-V diagram [33]

3.9 The concept of mean effective pressure

As stated above, the enclosed P-V diagram area is the work produced on the piston, in either the real or the ideal cycle. Fig 3.3 shows a second rectangular shaded area, equal in area to the enclosed cylinder P-V diagram. This rectangle is of height imep and of length V_{sv}, where imep is known as the indicated mean effective pressure and V_{sv} is the swept volume. The word "indicated" stems from the historical fact that pressure transducers for engines used to be called "indicator" and the P-V diagram, of a steam engine traditionally, was recorded on an "indicator card". The concept of mean effective pressure is extremely useful in relating one engine development to another for, while the units of imep are obviously that of pressure, the value is almost dimensionless. That remark is sufficiently illogical as to require careful explanation. The point is, any two engines of equal development or performance status will have identical values of mean effective pressure, even though they may be of totally dissimilar swept volume. In other words, Figs. 3.1, 3.2 and 3.3 could have equally well been plotted as pressure-compression (or volume) ratio and the values of imep would be identical for two engines of differing swept volume, if the diagrammatic profiles in the pressure direction were also identical [34].

3.10 Power, torque and fuel consumption

Power is defined as the rate of doing work. If the engine rotation rate is rps, revolutions per second, and the two-stroke engine has a working cycle per crankshaft revolution, then the power delivered to the piston crown by the gas is called the indicated power output, $\dot{W}_i$,

where:

$$\dot{W}_i = imep \times V_{sv} \times (work\ cycles\ per\ second)$$

$$= imep \times V_{sv}\, rps \qquad \text{- for a two-stroke engine} \qquad \text{(Eq. 3.25)}$$

$$= imep \times V_{sv} \times \frac{rps}{2} \qquad \text{- for a four-stroke engine}$$

For a four-stroke cycle engine, which has a working cycle lasting two crankshaft revolutions, the working cycle rate is 50% of the rps value, and this should be inserted into Eq. 3.25 rather than rps. In other words, a four-stroke cycle engine of equal power output and equal swept volume has an imep value which is double that of the two-stroke engine. Such is the actual, if somewhat illogical, convention used in everyday engineering practice.

The indicated torque, Z_i, is the turning moment on the crankshaft and is related to power output by the following equation:

$$\dot{W}_i = 2\,\pi\, Z_i\, rps \qquad \text{(Eq. 3.26)}$$

Should the engine actually consume fuel of calorific value C_{fl} at the measured (or at a theoretically calculated) mass flow rate of $\dot{m}_f$, then the indicated thermal efficiency, η_i, of the engine can be predicted from an extension of Eq. 3.23:

$$\eta_i = \frac{power\ output}{rate\ of\ heat\ input} = \frac{\dot{W}_i}{\dot{m}_f\, C_{fl}} \qquad \text{(Eq. 3.27)}$$

Of great interest and in common usage in engineering practice is the concept of specific fuel consumption, the fuel consumption rate unit power output. Hence, to continue the discussion on indicated values, indicated specific fuel consumption, isfc, is given by:

$$isfc = \frac{fuel\ consumption\ rate}{power\ output} = \frac{\dot{m}_f}{\dot{W}_i} \qquad \text{(Eq. 3.28)}$$

It will be observed from a comparison of Eqs. 3.27 and 3.28 that thermal efficiency and specific fuel consumption are reciprocally related to each other, without the employment of the calorific value of the fuel. As most petroleum-based have virtually identical values of calorific value, then the use of specific fuel consumption as a comparator from one engine to another, rather than thermal efficiency, is quite logical and is more immediately useful to the designer and the developer [35].

4 Turbulence modeling

If constant density and viscosity and no thermal interaction are assumed, the continuity and momentum equations are to be solved for velocity and pressure subject to no slip at the walls and known inlet and exit conditions.

Continuity: $$\frac{\partial u}{\partial x} + \frac{\partial v}{\partial y} + \frac{\partial w}{\partial z} = 0 \quad \text{(Eq. 4.1)}$$

Momentum: $$\rho \frac{\partial V}{\partial t} = -\nabla p + \rho g + \mu \nabla^2 V \quad \text{(Eq. 4.2)}$$

The differential energy relation is very important, both for heat transfer calculations and for general understanding of duct low processes. There is work being done by pressure forces to drive the fluid through the duct, where does this energy go? There is no work done by the wall shear stresses, because the velocity at the wall is zero. The answer is that pressure work is balanced by viscous dissipation in the interior of the flow. The integral of the dissipation function ϕ, over the flow field will equal the pressure work.

Both laminar and turbulent flows satisfy Eqs. 4.1 and 4.2 [36].

4.1 Reynolds' time averaging concept

For turbulent flow, because of the fluctuations, every velocity and pressure term in Eqs. 4.1 and 4.2 is a rapidly varying random function of time and space. At present our mathematics cannor handle such instantaneous fluctuating variables. No single pair of random functions V(x,y,z,t) and p(x,y,z,t) is known to be a solution to Eqs. 4.1 and 4.2. Moreover, our attentions as engineers is toward the average or mean values of velocity, pressure, shear stress, and the like in high-Reynols-number (turbulent) flow. This approach led Osborne Reynolds in 1895 to rewrite Eqs. 4.1 and 4.2 in terms of mean or time-averaged turbulent variables.

The time mean $\bar{u}$ of a turbulent function u(x,y,z,t) is defined by:

$$\bar{u} = \frac{1}{T}\int_0^T u\, dt \quad \text{(Eq. 4.3)}$$

where T is an averaging period taken to be longer than any significant period of the fluctuations themselves.

The fluctuation u' is defined as the deviation of u from its average value:

$$u' = u - \bar{u} \quad \text{(Eq. 4.4)}$$

It follows by definition that a fluctuation has zero mean value:

$$\overline{u'} = \frac{1}{T}\int_0^T (u - \bar{u})dt = \bar{u} - \bar{u} = 0 \quad \text{(Eq. 4.5)}$$

However, the mean square of a fluctuation is not zero and is a measure of the intensity of the turbulence:

$$\overline{u'^2} = \frac{1}{T}\int_0^T u'^2 dt \neq 0 \quad \text{(Eq. 4.6)}$$

Nor in general are the mean fluctuation products such as $\overline{u'v'}$ and $\overline{u'p'}$ zero in a typical turbulent flow.

Reynolds's idea was to split each property into mean plus fluctuating variables:

$$u = \bar{u} + u' \quad v = \bar{v} + v' \quad w = \bar{w} + w' \quad p = \bar{p} + p' \tag{Eq. 4.7}$$

Substitute these into Eqs. 4.1 and 4.2, and take the time mean of each equation. The continuity relation reduces to

$$\frac{\partial \bar{u}}{\partial x} + \frac{\partial \bar{v}}{\partial y} + \frac{\partial \bar{w}}{\partial z} = 0 \tag{Eq. 4.8}$$

which is no different from a laminar continuity relation.

However, each component of the momentum equation (4.2), after time averaging, will contain mean values plus three mean products, or correlations, of fluctuating velocities. The most important of these is the momentum relation in the mainstream, or x, direction, which takes the form:

$$\rho \frac{d\bar{u}}{dt} = -\frac{\partial \bar{p}}{\partial x} + \rho g_x + \frac{\partial}{\partial x}\left(\mu \frac{\partial \bar{u}}{\partial x} - \rho\overline{u'^2}\right) + \frac{\partial}{\partial y}\left(\mu \frac{\partial \bar{u}}{\partial y} - \rho\overline{u'v'}\right) + \frac{\partial}{\partial z}\left(\mu \frac{\partial \bar{u}}{\partial z} - \rho\overline{u'w'}\right) \tag{Eq. 4.9}$$

The three correlation terms $-\rho\overline{u'^2}$, $-\rho\overline{u'v'}$, and $-\rho\overline{u'w'}$ called turbulent stresses because they have the same dimensions and occur right alongside the Newtonian (laminar) stress terms $\mu(\partial\bar{u}/\partial x)$ and so on. Actually, they are convective acceleration terms (which is why the density appears), not stresses, but they have the mathematical effect of stress and are so termed almost universally in the literature.

The turbulent stresses are unknown a priori and must be related by experiment to geometry and flow conditions. Fortunately, in duct and boundary layer flow, the stress $-\rho\overline{u'v'}$, associated with direction y normal to the wall is dominant, and approximate with excellent accuracy a simpler streamwise momentum equation can be approximated:

$$\rho \frac{d\bar{u}}{dt} \approx -\frac{\partial \bar{p}}{\partial x} + \rho g_x + \frac{\partial \tau}{\partial y} \tag{Eq. 4.10}$$

where;

$$\tau = \mu \frac{\partial \bar{u}}{\partial y} - \rho\overline{u'v'} = \tau_{lam} + \tau_{turb} \tag{Eq. 4.11}$$

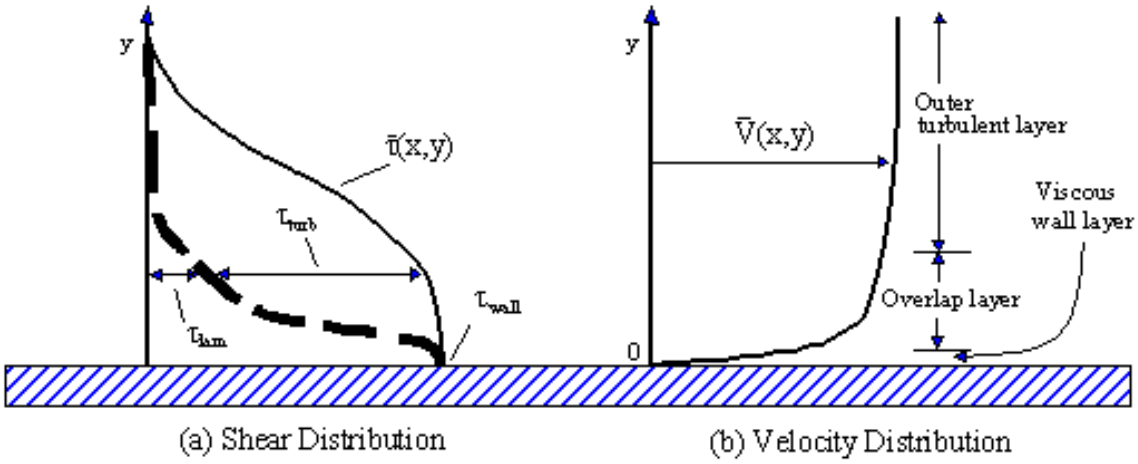

Fig. 4.1 Typical velocity and shear distributions in turbulent flow near a wall [37]

Fig. 4.1 shows the distribution of τ_{lam} and τ_{turb} from typical measurements across a turbulent shear layer near wall. Laminar shear is dominant near the wall (the wall layer), and turbulent shear dominates in the outer layer. There is an intermediate region, called the overlap layer, where both laminar and turbulent shear are important. These three regions are labeled in Fig. 4.1.

In the outer layer τ_{turb} is two or three orders of magnitude greater than τ_{lam}, and vice versa in the wall layer. These experimental facts enable us to use a crude but very effective model for the velocity distribution $\bar{u}(y)$ across a turbulent wall layer [37].

4.2 The logarithmic overlap law

There are three regions in turbulent flow near a wall that has been seen in Fig. 4.1:

1. Wall layer: Viscous shear dominates.
2. Outer layer: Turbulent shear dominates.
3. Overlap layer: Both types of shear are important.

From now on let us agree to drop the overbar from velocity $\bar{u}$. Let τ_w be the wall shear stress, and let δ and U represent the thickness and velocity at the edge of the outer layer, y=δ.

For the wall layer, Prandtl deduced in 1930 that u must be independent of the shear layer thickness:

$$u = f(\mu, \tau_w, \rho, y) \qquad \text{(Eq. 4.12)}$$

By dimensional analysis, this is equivalent to:

$$u^+ = \frac{u}{u^*} = F\left(\frac{yu^*}{u}\right) \quad u^* = \left(\frac{\tau_w}{\rho}\right)^{1/2} \qquad \text{(Eq. 4.13)}$$

Eq. 4.13 is called the law of the wall, and the quantity u^* is termed the friction velocity because it has dimensions $[LT^{-1}]$, although it is not actually a flow velocity.

Subsequently, Kármán in 1933 deduced that u in the outer layer is independent of molecular viscosity, but its deviation from the stream velocity U must depend on the layer thickness δ and other properties:

$$(U-u)_{outer} = g(\delta, \tau_w, \rho, y) \quad \text{(Eq. 4.14)}$$

Again, by dimensional analysis we this is rewrite as:

$$\frac{U-u}{u^*} = G\left(\frac{y}{\delta}\right) \quad \text{(Eq. 4.15)}$$

where u^* has the same meaning as in Eq. 4.13. Eq. 4.15 is called the velocity defect law for the outer layer.

Both the wall law 4.13 and the defect law 4.15 are found to be accurate for a wide variety of experimental turbulent duct and boundary layer [1 to 3]. They are different in form, yet they must overlap smoothly in the intermediate layer. In 1937 C. B. Millikan showed that this can be true only if the overlap layer velocity varies logarithmically with y:

$$\frac{u}{u^*} = \frac{1}{K} ln \frac{yu^*}{v} + B \qquad \text{overlap layer} \quad \text{(Eq. 4.16)}$$

Over the full range of turbulent smooth wall flows, the dimensionless constants K and B are found to have the approximate values $K \approx 0.41$ and $B \approx 5.0$. Eq. 4.16 is called the logarithmic overlap layer.

Thus by dimensional reasoning and physical insight, a plot of u versus lny that is inferred in a turbulent shear layer will show a curved wall region, a curved outer region, and a straight-line logarithmic overlap.

The wall law is unique and follows the linear viscous relation

$$u^+ = \frac{u}{u^*} = \frac{yu^*}{v} = y^+ \quad \text{(Eq. 4.17)}$$

from the wall to about $y^+ = 5$, thereafter curving over to merge with logarithmic law at about $y^+ = 30$.

The logarithmic law (4.16), instead of just being a short overlapping link, actually approximates nearly the entire velocity profile, except for the outer law when the pressure is increasing strongly downstream (as in a diffuser). The inner wall law typically extends over less than 2 percent of the profile and can be neglected. Thus Eq. 4.16 can be used as an excellent approximation to solve nearly every turbulent flow problem [38].

4.3 Advanced modeling concepts

Turbulence modeling is a very active field. Scores of papers have been published to more accurately simulate the turbulent stresses in Eq. 4.9 and their y and z components. For example, L, Prandtl, who invented boundary layer theory in 1904, later proposed an eddy viscosity model of the Reynolds stress term in Eq. 4.12:

$$-\rho\overline{u'v'} = \tau_{turb} = \mu_1 \frac{du}{dy} \quad \text{where} \quad \mu_1 \approx \rho l^2 \left|\frac{du}{dy}\right| \qquad \text{(Eq. 4.18)}$$

The term μ_1, which is a property of the flow, not the fluid, is called the eddy viscosity and can be modeled in various ways. The most popular form is Eq. 4.12, where l is called the mixing length of the turbulent eddies (analogous to mean free path in molecular theory). Near a solid wall, l is approximately proportional to distance from the wall, and Kármán suggested.

$$l \approx Ky \quad \text{where} \quad \text{K= Kármán's constant} \approx 0.41 \qquad \text{(Eq. 4.19)}$$

Modern turbulence models approximate three-dimensional turbulent flows and employ additional partial differential equations for such quantities as the turbulence kinetic energy, the turbulent dissipation, and the six Reynolds stresses [39].

4.4 Turbulence: some important thoughts

"Most flows occurring in nature and in engineering applications are turbulent. The boundary layer in the earth's atmosphere is turbulent (except possibly in very stable conditions); jet streams in the upper troposphere are turbulent; cumulus clouds are in turbulent motion. The water currents below the surface of the oceans are turbulent; the Gulf Stream is a turbulent wall-jet kind of flow. The photosphere of the sun and the photospheres of similar stars are in turbulent motion; interstellar gas clouds (gaseous nebulae) are turbulent; the wake of the earth in the solar wind is presumably a turbulent wake. Boundary layers growing on aircraft wings are turbulent. Most combustion processes involve turbulence and even depend on it; the flow of natural gas and oil in pipelines is turbulent. Chemical engineers use turbulence to mix and homogenize fluid mixtures and to accelerate chemical reaction rates in liquids or gases. The flow of water in rivers and canals is turbulent; the wakes of ships, cars, submarines and aircraft are in turbulent motion. The study of turbulence is clearly an interdisciplinary activity, which has a very wide range of applications. In fluid dynamics laminar flow is the exception, not the rule: one must have small dimensions and high viscosities to encounter laminar flow."

Turbulence have been discussed without offering any actual definition for it, because the turbulence is resistant to precise definition. Instead, the following properties have been mentioned.

- **High Reynolds number.** Turbulence occurs at high Reynolds number. Remember that instability of laminar flow was one way that flows become turbulent; instability of a particular flow requires that the Reynolds number exceed come minimum value. The high Reynolds number also means that at the large scales of the flow, inertial forces dominate over viscous forces.
- **Randomness and disorder.** Turbulent flows exhibit a high degree of randomness and disorder, particularly at small scales. These random fluctuations are described by decomposing the flow variables into mean and fluctuating parts, e.g. $u_i = \bar{u}_i + u'_i$.
- **Disparity in length scales.** A wide range of length scales are relevant in turbulent flows. The spread between the largest and smallest length scales in a flow increases with increasing Reynolds number. This makes computation extremely difficult.

- **Energy cascade.** In a turbulent flow, energy generally gets transferred from the large scales to the small scales in an inviscid fashion, and then gets dissipated at the small scales by the action of viscosity. The pressure of dissipation in turbulent flows is significant; even though the large flow scales may be essentially inviscid, there is viscous dissipation of kinetic energy going on in the flow, at the scales.
- **Increased transport of momentum, scalar etc.** The random fluctuations of turbulent flows provide another mechanism by which quantities can get transferred from one portion of a flow to another. In a laminar flow, transport of momentum mostly occurs through viscosity (diffusion), while in a turbulent flow, transport can occur through the random motion embodied by the fluctuating terms. Think of a parallel flow, with all the (mean) velocity vectors pointing in the same direction (say, the x-direction). In the laminar case, momentum only gets transferred between layers by viscous drag. In the turbulent case, however, there can be velocity fluctuations in the y-direction to carry momentum across the mean streamlines [40].

5 The Navier Stokes equations

5.1 Derivation of the Navier Stokes equations

Here, an approach is outlined for obtaining the Navier Stokes equations that builds on the methods used in earlier years of applying mass conservation and force-momentum principles to a control volume.

The approach involves:

- Defining a small control volume within the flow.
- Applying the mass conservation and force-momentum principle to the control volume.
- Considering what happens in the limit as the control volume becomes infinitesimally small.

Although the derivation can be done using any arbitrarily shaped control volume, for simplicity, a rectangular control volume is considered here.
The equations will be first derived for two-dimensional, unsteady, flow conditions, and it should then be apparent how these extend to three-dimensional flows [41].

5.2 Mass conservation (continuity)

The mass conservation principle is:

$$\begin{bmatrix} Rate\ of\ mass \\ accumulation\ within\ CV \end{bmatrix} = \begin{bmatrix} Rate\ of\ mass \\ flow\ into\ CV \end{bmatrix} - \begin{bmatrix} Rate\ of\ mass \\ flow\ out\ of\ CV \end{bmatrix} \quad \text{(Eq. 5.1)}$$

For a two-dimensional control volume of dimensions Δx and Δy as shown in (Fig. 5.1):

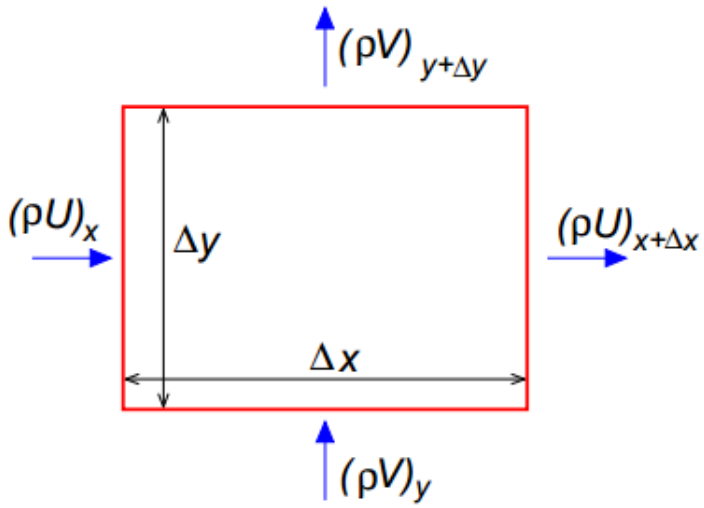

Fig. 5.1 Two dimensional control volume [41]

$$Mass\ accumulation\ rate\ =\ \partial(\rho\Delta x\Delta y)/\partial t \qquad \text{(Eq. 5.2)}$$

$$Mass\ inflow\ =\ (\rho U)_{x^{\Delta y}} + (\rho V)_{y^{\Delta x}} \qquad \text{(Eq. 5.3)}$$

$$Mass\ outflow\ =\ (\rho U)_{x+\Delta x^{\Delta y}}\ + (\rho V)_{y+\Delta y^{\Delta x}} \qquad \text{(Eq. 5.4)}$$

The mass conservation equation thus gives:

$$\frac{\partial(\rho\Delta x\Delta y)}{\partial t} =\ (\rho U)_{x^{\Delta y}}\ + (\rho V)_{y^{\Delta x}}\ - (\rho U)_{x+\Delta x^{\Delta y}}\ - (\rho V)_{y+\Delta y^{\Delta x}} \qquad \text{(Eq. 5.5)}$$

Division by ΔxΔy and rearrangement leads to:

$$\frac{\partial\rho}{\partial t} = \frac{(\rho U)_x - (\rho U)_{x+\Delta x}}{\Delta x} + \frac{(\rho V)_y - (\rho V)_{y+\Delta y}}{\Delta y} \qquad \text{(Eq. 5.6)}$$

In the limit as Δx, Δy → 0, the control volume becomes infinitesimally small, and using Taylor series expansions that is had:

$$(\rho U)_{x+\Delta x} \rightarrow (\rho U)_x + \Delta x\frac{\partial(\rho U)}{\partial x} \quad (\rho V)_{y+\Delta y} \rightarrow\ (\rho V)_y + \Delta y\frac{\partial(\rho V)}{\partial y} \qquad \text{(Eq. 5.7)}$$

Substituting these into Eq. 5.6 gives:

$$\frac{\partial\rho}{\partial t} = -\frac{\partial(\rho U)}{\partial x} - \frac{\partial(\rho V)}{\partial y} \quad \text{or} \quad \frac{\partial\rho}{\partial t} + \frac{\partial(\rho U)}{\partial x} + \frac{\partial(\rho V)}{\partial y} = 0 \qquad \text{(Eq. 5.8)}$$

In three-dimensional flows this is easily extended to:

$$\frac{\partial\rho}{\partial t} + \frac{\partial(\rho U)}{\partial x} + \frac{\partial(\rho V)}{\partial y} + \frac{\partial(\rho W)}{\partial z} = 0 \qquad \text{(Eq. 5.9)}$$

In steady-state flows, $\partial\rho/\partial t = 0$, so:

$$\frac{\partial(\rho U)}{\partial x} + \frac{\partial(\rho V)}{\partial y} + \frac{\partial(\rho W)}{\partial z} = 0 \qquad \text{(Eq. 5.10)}$$

In incompressible flows the density is constant, so that is obtained [41]:

$$\frac{\partial U}{\partial x} + \frac{\partial V}{\partial y} + \frac{\partial W}{\partial z} = 0 \qquad \text{(Eq. 5.11)}$$

5.3 Force-momentum principle

The force momentum principle is:

$$\begin{bmatrix} Accumulation\ of\ momentum \\ with\ in\ CV \end{bmatrix} = \begin{bmatrix} Rate\ of\ momentum \\ flow\ into\ CV \end{bmatrix} - \begin{bmatrix} Rate\ of\ momentum \\ flow\ out\ of\ CV \end{bmatrix} + \begin{bmatrix} Forces\ acting \\ on\ CV\ faces \end{bmatrix} + \begin{bmatrix} Body\ forces \\ within\ CV \end{bmatrix} \qquad \text{(Eq. 5.12)}$$

Consider the U momentum equation, on a control volume of dimensions Δx and Δy:

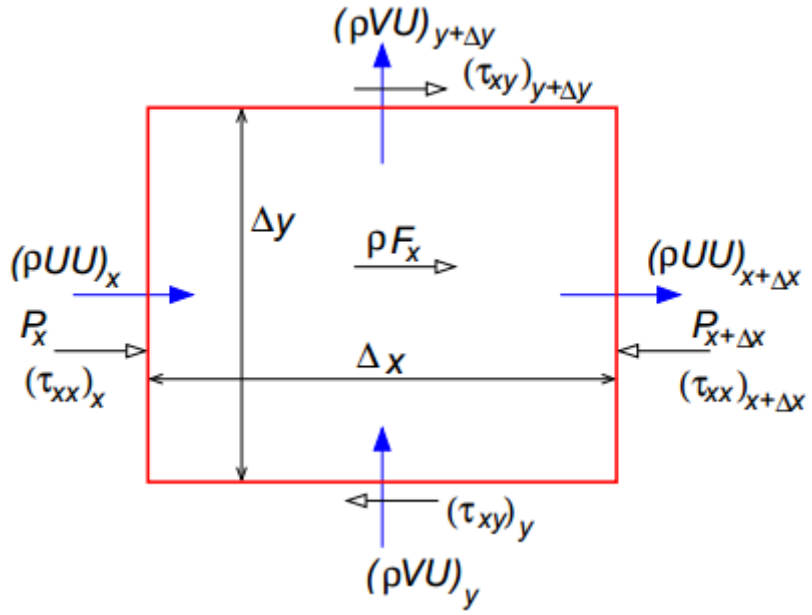

Fig. 5.2 Control volume [41]

$$Accumulation\ rate\ =\ \Delta x \Delta y\ [\frac{\partial(\rho U)}{\partial t}] \qquad \text{(Eq. 5.13)}$$

$$Mom.\ flux\ in = \Delta y(\rho UU)_x + \Delta x(\rho VU)_y \qquad \text{(Eq. 5.14)}$$

$$Mom.\ flux\ out\ =\ \Delta y(\rho UU)_{x+\Delta x} + \Delta x(\rho VU)_{y+\Delta y} \qquad \text{(Eq. 5.15)}$$

Surface forces arise from the pressure and viscous stresses:

$$Net\ surface\ force = [(P + \tau_{xx})_x - (P + \tau_{xx})_{x+\Delta x}]\Delta y + [(\tau_{xy})_y - (\tau_{xy})_{y+\Delta y}]\Delta x \quad \text{(Eq. 5.16)}$$

$$Body\ force = \rho F_x \Delta x \Delta y \quad \text{(Eq. 5.17)}$$

The U-momentum balance then gives:

$$\Delta x \Delta y \left[\frac{\partial(\rho U)}{\partial t}\right] = [(\rho UU)_x - (\rho UU)_{x+\Delta x}]\Delta y + [(\rho VU)_y - (\rho VU)_{y+\Delta y}]\Delta x + [(P + \tau_{xx})_x - (P + \tau_{xx})_{x+\Delta x}]\Delta y + [(\tau_{xy})_y - (\tau_{xy})_{y+\Delta y}]\Delta x + \rho F_x \Delta x \Delta y \quad \text{(Eq. 5.18)}$$

Dividing by ΔxΔy gives:

$$\frac{\partial(\rho U)}{\partial t} = \frac{(\rho UU)_x - (\rho UU)_{x+\Delta x}}{\Delta x} + \frac{(\rho VU)_y - (\rho VU)_{y+\Delta y}}{\Delta y} + \frac{P_x - P_{x+\Delta x}}{\Delta x} + \frac{(\tau_{xx})_x - (\tau_{xx})_{x+\Delta x}}{\Delta x} + \frac{(\tau_{xy})_y - (\tau_{xy})_{y+\Delta y}}{\Delta y} + \rho F_x \quad \text{(Eq. 5.19)}$$

As before, as Δx and Δy → 0, for any quantity φ we have:

$$\varphi_{x+\Delta x} \to \varphi_x + \Delta x \frac{\partial \varphi}{\partial x} \quad \text{and} \quad \varphi_{y+\Delta y} \to \varphi_y + \Delta y \frac{\partial \varphi}{\partial y} \quad \text{(Eq. 5.20)}$$

Applying the terms in Eq. 5.20 to Eq. 5.19 the U-momentum balance becomes:

$$\frac{\partial(\rho U)}{\partial t} = -\frac{\partial(\rho UU)}{\partial x} - \frac{\partial(\rho VU)}{\partial y} - \frac{\partial P}{\partial x} - \frac{\partial \tau_{xx}}{\partial x} - \frac{\partial \tau_{xy}}{\partial y} + \rho F_x \quad \text{(Eq. 5.21)}$$

Rearranging gives the usual form of the U-momentum equation:

$$\frac{\partial(\rho U)}{\partial t} + \frac{\partial(\rho U^2)}{\partial x} + \frac{\partial(\rho VU)}{\partial y} = -\frac{\partial P}{\partial x} - \frac{\partial \tau_{xx}}{\partial x} - \frac{\partial \tau_{xy}}{\partial y} + \rho F_x \quad \text{(Eq. 5.22)}$$

As with the continuity equation, the U momentum equation is also a differential equation.

The corresponding V-momentum equation is:

$$\frac{\partial(\rho V)}{\partial t} + \frac{\partial(\rho UV)}{\partial x} + \frac{\partial(\rho V^2)}{\partial y} = -\frac{\partial P}{\partial y} - \frac{\partial \tau_{xy}}{\partial x} - \frac{\partial \tau_{yy}}{\partial y} + \rho F_y \quad \text{(Eq. 5.23)}$$

In their above forms, however, the U and V-momentum equations still contain additional unknown variables, namely the viscous stresses, τ_{xx}, τ_{yy} and τ_{xy} [41].

5.4 The viscous stresses

In a simple shear flow, Stoke's law states that the viscous shear stress, τ_{xy}, is obtained from:

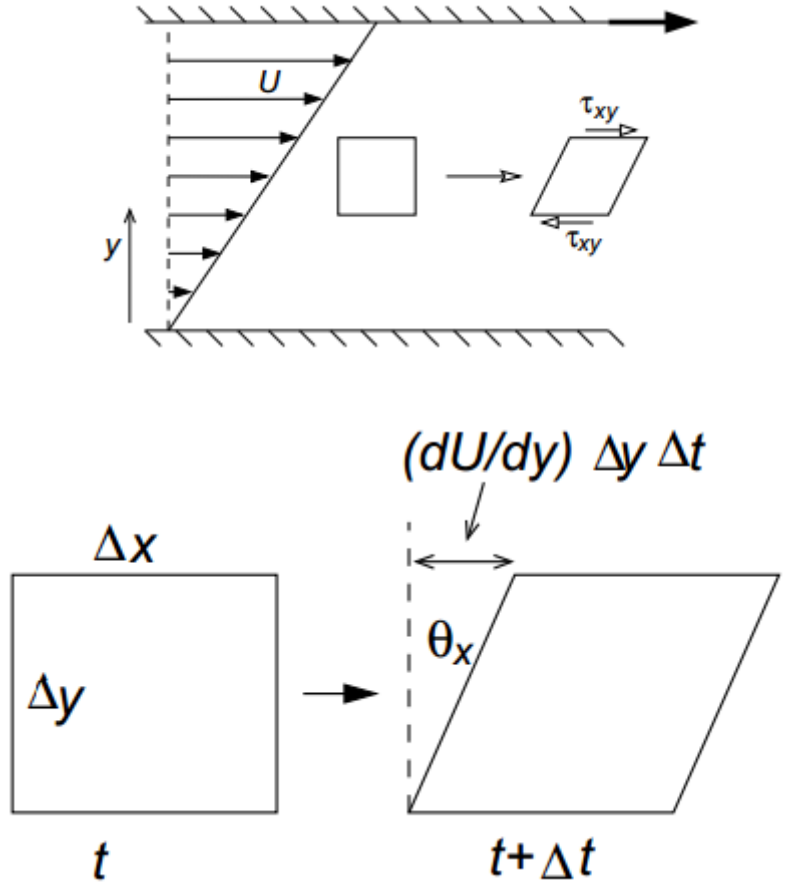

Fig. 5.3 Viscous shear stress [41]

$$\tau_{xy} = -\mu \frac{\partial U}{\partial y} \qquad \text{(Eq. 5.24)}$$

This equation can be obtained by considering how, in a simple case, the rate at which a fluid element is deformed is opposed by the fluid viscosity.

$$tan(\theta_x) = \frac{(\partial U/\partial y)\Delta y \Delta t}{\Delta y} \qquad \text{(Eq. 5.25)}$$

For small θx, tan(θx) ≈ θx, so; $\frac{\partial \theta_x}{\partial t} \approx \frac{\partial U}{\partial y}$

For many common fluids we have $\tau \propto \partial\theta_x/\partial t$.

In the more general case, expressions for the viscous stresses can again be derived by considering the deformation caused by the flow field to an initially rectangular fluid element.

For Newtonian fluids these general stress-strain relations can be expressed as the viscous stresses being linearly related to the strain rates, with the constant of proportionality being the viscosity μ.

Hence, in 2-D, the viscous stresses are obtained a:

$$\tau_{xx} = -2\mu\frac{\partial U}{\partial x} \qquad \tau_{yy} = -2\mu\frac{\partial V}{\partial y} \qquad \tau_{xy} = -\mu\left(\frac{\partial U}{\partial x} + \frac{\partial V}{\partial x}\right) \tag{Eq. 5.26}$$

Substituting the expressions for τ_{xx} and τ_{xy} into the U momentum equation gives:

$$\frac{\partial(\rho U)}{\partial t} + \frac{\partial(\rho U^2)}{\partial x} + \frac{\partial(\rho VU)}{\partial y} = -\frac{\partial P}{\partial x} + \frac{\partial}{\partial x}\left[2\mu\frac{\partial U}{\partial x}\right] + \frac{\partial}{\partial y}\left[\mu\left(\frac{\partial U}{\partial y} + \frac{\partial V}{\partial x}\right)\right] + \rho F_x \tag{Eq. 5.27}$$

A similar equation can be derived for the V momentum component [41].

5.5 The Navier Stokes equations

The above set of equations that describe a real fluid motion are collectively known as the Navier Stokes equations. In 2-D they can be written as:

The continuity equation:

$$\frac{\partial\rho}{\partial t} + \frac{\partial(\rho U)}{\partial x} + \frac{\partial(\rho V)}{\partial y} = 0 \tag{Eq. 5.28}$$

The U-momentum equation:

$$\frac{\partial(\rho U)}{\partial t} + \frac{\partial(\rho U^2)}{\partial x} + \frac{\partial(\rho VU)}{\partial y} = -\frac{\partial P}{\partial x} + \frac{\partial}{\partial x}\left[2\mu\frac{\partial U}{\partial x}\right] + \frac{\partial}{\partial y}\left[\mu\left(\frac{\partial U}{\partial y} + \frac{\partial V}{\partial x}\right)\right] + \rho F_x \tag{Eq. 5.29}$$

The V-momentum equation:

$$\frac{\partial(\rho U)}{\partial t} + \frac{\partial(\rho UV)}{\partial x} + \frac{\partial(\rho V^2)}{\partial y} = -\frac{\partial P}{\partial x} + \frac{\partial}{\partial x}\left[\mu\left(\frac{\partial V}{\partial x} + \frac{\partial U}{\partial y}\right)\right] + \frac{\partial}{\partial y}\left[2\mu\frac{\partial V}{\partial y}\right] + \rho F_y \tag{Eq. 5.30}$$

In three-dimensional flows the equations are expanded to [41]:

Continuity:

$$\frac{\partial\rho}{\partial t} + \frac{\partial(\rho U)}{\partial x} + \frac{\partial(\rho V)}{\partial y} + \frac{\partial(\rho W)}{\partial z} = 0 \tag{Eq. 5.31}$$

U-momentum:

$$\frac{\partial(\rho U)}{\partial t} + \frac{\partial(\rho U^2)}{\partial x} + \frac{\partial(\rho VU)}{\partial y} + \frac{\partial(\rho WU)}{\partial z} = -\frac{\partial P}{\partial x} + 2\frac{\partial}{\partial x}\left[\mu\frac{\partial U}{\partial x}\right] + \frac{\partial}{\partial y}\left[\mu\left(\frac{\partial U}{\partial y} + \frac{\partial V}{\partial x}\right)\right] + \frac{\partial}{\partial z}\left[\mu\left(\frac{\partial V}{\partial z} + \frac{\partial W}{\partial y}\right)\right] + \rho F_x \tag{Eq. 5.32}$$

V-momentum:

$$\frac{\partial(\rho V)}{\partial t} + \frac{\partial(\rho UV)}{\partial x} + \frac{\partial(\rho VV)}{\partial y} + \frac{\partial(\rho WV)}{\partial z} = -\frac{\partial P}{\partial y} + \frac{\partial}{\partial x}\left[\mu\left(\frac{\partial V}{\partial x} + \frac{\partial U}{\partial y}\right)\right] + 2\frac{\partial}{\partial y}\left[\mu\frac{\partial V}{\partial y}\right] + \frac{\partial}{\partial z}\left[\mu\left(\frac{\partial V}{\partial z} + \frac{\partial W}{\partial y}\right)\right] + \rho F_y \tag{Eq. 5.33}$$

W-momentum :

$$\frac{\partial(\rho W)}{\partial t}+\frac{\partial(\rho UW)}{\partial x}+\frac{\partial(\rho VW)}{\partial y}+\frac{\partial(\rho WW)}{\partial z}=-\frac{\partial P}{\partial z}+\frac{\partial}{\partial x}\left[\mu\left(\frac{\partial W}{\partial x}+\frac{\partial U}{\partial z}\right)\right]+\frac{\partial}{\partial y}\left[\mu\left(\frac{\partial W}{\partial y}+\frac{\partial V}{\partial z}\right)\right]+ 2\frac{\partial}{\partial z}\left[\mu\frac{\partial W}{\partial z}\right]+\rho F_z \quad \text{(Eq. 5.34)}$$

5.6 Convection and diffusion terms

The term $\frac{\partial(\rho U\varphi)}{\partial x}+\frac{\partial(\rho V\varphi)}{\partial y}+\frac{\partial(\rho W\varphi)}{\partial z}$ where φ stands for any of the velocity components (U, V or W) represents convection of φ by the fluid. The terms on the right hand sides of the equations involving the viscosity represent viscous diffusion.

The general form of the momentum transport equations is thus seen to be:

Time derivative+Convection terms = Forcing terms+Diffusion terms

The combination of time derivative and convection terms represents the total rate of change of a quantity following a fluid path line. It is often written in shorthand notation as Dφ/Dt:

$$\frac{D\varphi}{Dt}\equiv\frac{\partial\varphi}{\partial t}+\frac{\partial(U\varphi)}{\partial x}+\frac{\partial(V\varphi)}{\partial y}+\frac{\partial(W\varphi)}{\partial z} \quad \text{(Eq. 5.35)}$$

The time derivative and convection terms are sometimes written as above (with ρ, U, V, W inside the derivatives), and sometimes in the form:

$$\rho\frac{\partial\varphi}{\partial t}+\rho U\frac{\partial\varphi}{\partial x}+\rho V\frac{\partial\varphi}{\partial y}+\rho W\frac{\partial\varphi}{\partial z}$$

These are, in fact, entirely equivalent, since differentiating by parts gives:

$$\frac{\partial\rho\varphi}{\partial t}+\frac{\partial\rho U\varphi}{\partial x}+\frac{\partial\rho V\varphi}{\partial y}+\frac{\partial\rho W\varphi}{\partial z}=\rho\frac{\partial\varphi}{\partial t}+\varphi\frac{\partial\rho}{\partial t}+\rho U\frac{\partial\varphi}{\partial x}+\varphi\frac{\partial\rho U}{\partial x}+\rho V\frac{\partial\varphi}{\partial y}+\varphi\frac{\partial\rho V}{\partial y}+\rho W\frac{\partial\varphi}{\partial z}+ \varphi\frac{\partial\rho W}{\partial z}=\rho\frac{\partial\varphi}{\partial t}+\rho U\frac{\partial\varphi}{\partial x}+\rho V\frac{\partial\varphi}{\partial y}+\rho W\frac{\partial\varphi}{\partial z}+\varphi\left(\frac{\partial\rho}{\partial t}+\frac{\partial\rho U}{\partial x}+\frac{\partial\rho V}{\partial y}+\frac{\partial\rho W}{\partial z}\right) \quad \text{(Eq. 5.36)}$$

and the term in brackets multiplied by φ is zero from the continuity equation.

If the viscosity is constant the diffusion terms can be simplified by taking μ outside the derivatives. In 2-D [41], for example:

$$2\frac{\partial}{\partial x}\left[\mu\frac{\partial U}{\partial x}\right]+\frac{\partial}{\partial y}\left[\mu\left(\frac{\partial U}{\partial y}+\frac{\partial V}{\partial x}\right)\right]=\mu\frac{\partial}{\partial x}\left[\frac{\partial U}{\partial x}\right]+\mu\frac{\partial}{\partial y}\left[\frac{\partial U}{\partial y}\right]+\mu\frac{\partial}{\partial x}\left[\frac{\partial U}{\partial x}\right]+\mu\frac{\partial}{\partial y}\left[\frac{\partial V}{\partial x}\right]=\mu\frac{\partial^2U}{\partial x^2}+ \mu\frac{\partial^2U}{\partial y^2}+\mu\frac{\partial}{\partial x}\left[\frac{\partial U}{\partial y}+\frac{\partial V}{\partial x}\right]=\mu\frac{\partial^2U}{\partial x^2}+\mu\frac{\partial^2U}{\partial y^2} \quad \text{(Eq. 5.37)}$$

5.7 Further simplification

In many flows that will be considered certain additional simplifications can be introduced.
In steady flows the time derivatives become zero:

$$\frac{\partial(\rho U)}{\partial t} = \frac{\partial(\rho V)}{\partial t} = \frac{\partial(\rho W)}{\partial t} = 0 \qquad \text{(Eq. 5.38)}$$

The body force terms, F_x, F_y, F_z, are, in many cases, negligible.

These simplifications lead to the momentum equations for a 2-D steady, incompressible, constant viscosity [41], flow without body forces being given by:

$$\rho\frac{\partial(U^2)}{\partial x} + \rho\frac{\partial(VU)}{\partial y} = -\frac{\partial P}{\partial x} + \mu\frac{\partial^2(U)}{\partial x^2} + \mu\frac{\partial^2(U)}{\partial y^2} + \rho\frac{\partial(UV)}{\partial x} + \rho\frac{\partial(V^2)}{\partial y} = -\frac{\partial P}{\partial x} + \mu\frac{\partial^2 U}{\partial x^2} + \mu\frac{\partial^2 V}{\partial y^2} \qquad \text{(Eq. 5.39)}$$

5.8 Other transport equations

The governing equations for other quantities transported by a flow often take the same general form of transport equation to the above momentum equations.
For example, the transport equation for the evolution of temperature in a fluid flow can often be written (in 2-D for simplicity) as:

$$\frac{\partial T}{\partial t} + \frac{\partial(UT)}{\partial x} + \frac{\partial(VT)}{\partial y} = \frac{\partial}{\partial x}\left(\alpha\frac{\partial T}{\partial x}\right) + \frac{\partial}{\partial y}\left(\alpha\frac{\partial T}{\partial y}\right) \qquad \text{(Eq. 5.40)}$$

where α is the molecular thermal diffusivity [41].

5.9 Solving the Naiver Stokes equations

The Navier Stokes equations form a system of differential equations:

- In two-dimensional flows there are three variables (U, V, P) and three differential equations (Continuity, U and V-momentum).
- In three-dimensional flows there are four variables and four differential equations.

Although the equations have been presented for a Cartesian coordinate system (x, y, z), they can also be transformed mathematically to other coordinate systems, (eg. cylindrical, or spherical, polars).

In principle, therefore, the Navier Stokes equations can be integrated over a flow domain of interest, with appropriate boundary conditions, to produce detailed velocity and pressure fields.

Although analytical solutions can be obtained for a few cases, in practice the equations must usually be solved using **numerical methods**. So, in this project a program has been used can solve these equations [41].

5.10 Analytical solutions of the Navier Stokes equations

There are a few, very simple, laminar flows for which the Navier Stokes equations can be solved analytically.

For example, for steady, incompressible, fully developed flow in a plane channel, we have V = 0 and U does not depend on x.

Continuity ($\partial U/\partial x + \partial V/\partial y = 0$) is satisfied.

The V momentum equation reduces to $\partial P/\partial y = 0$, so P is constant across the channel.

The U momentum equation becomes:

$$0 = -\frac{\partial P}{\partial x} + \frac{\partial}{\partial y} + \left(\mu \frac{\partial U}{\partial y}\right) \quad \text{(Eq. 5.41)}$$

with boundary conditions U = 0 at y = ±h .

Since P is not a function of y, that can be easily integrate this:

$$\mu \frac{\partial U}{\partial y} = y \frac{\partial P}{\partial x} + A \quad \text{(Eq. 5.42)}$$

for some constant of integration A. Integrating a second time gives:

$$\mu U = \frac{y^2}{2} \frac{\partial P}{\partial x} + Ay + B \quad \text{(Eq. 5.43)}$$

To determine the constants A and B, the boundary conditions are applied that U = 0 at y = ±h:

$$0 = \frac{h^2}{2} \frac{\partial P}{\partial x} + Ah + B \qquad \text{and} \qquad 0 = \frac{h^2}{2} \frac{\partial P}{\partial x} - Ah + B \quad \text{(Eq. 5.44)}$$

The velocity profile is therefore given by the parabola

$$U = -\frac{1}{2\mu} \frac{\partial P}{\partial x} (h^2 - y^2) \quad \text{(Eq. 5.45)}$$

The pressure gradient can be related to the bulk (average) velocity, since:

$$U_b = \frac{1}{2h} \int_{-h}^{h} U(y) dy = -\frac{1}{4h\mu} \frac{\partial P}{\partial x} \int_{-h}^{h} (h^2 - y^2) dy = -\frac{1}{4h\mu} \frac{\partial P}{\partial x} \left[h^2 y - \frac{y^3}{3} \right]_{-h}^{h} = -\frac{h^2}{3\mu} \frac{\partial P}{\partial x} \quad \text{(Eq. 5.46)}$$

Hence $\partial P/\partial x = -3\mu U_b/h^2$, and the velocity profile can be written as:

$$U = (3/2) U_b (1 - y^2/h^2) \quad \text{(Eq. 5.47)}$$

A similar analysis can be applied to some other simple 1-D flows, such as fully-developed pipe flow, flow between moving infinite flat plates, etc. However, for a turbulent flow you should use numerical solution [41].

6 Commercial CFD solver

This is a three-dimensional fluid dynamics program which has been used for modeling cold flow in cylinder that has been developed specifically to address fluid flow simulations in the vehicle and engine industries. That is developed around a completely automatic mesh generator, providing a rapid turnaround time for CFD analyses. The fully automatic mesh generator, unique to this Commercial CFD Solver, provides a distinct advantage over most other commercial CFD tools; in that it ensures CFD is an integral part of modern engineering development programs [42].

6.1 Applications

- **In-cylinder air motion and mixture preparation**
- Spray dynamics
- Combustion modelling
- Intake system component design and optimisation
- Exhaust system component development, exhaust gas recirculation, catalyst optimisation and exhaust muffler development
- Coupled 1D/3D simulations for more accurate transient results
- Coolant circuit design and development
- Advanced thermal management using conjugate heat transfer, radiation and transient simulations allows hot soak, thermal shock and warm-up simulations
- Vehicle thermal management simulations

6.2 Key features

- Fully automatic mesh generator capable of 500,000 cells/hr
- Boolean operations for automatic joining, intersection or subtraction of different geometric entities
- Geometry wrapper for fast repair of poor quality input data
- Easy to use/flexible mesh motion definition
- Intuitive and easy to use GUIs
- Appropriate sub-models for automotive applications
- Advanced fuel spray and combustion models
- Internal/External injector flow coupling
- Fan model for radial and axial fans of varying complexity
- Steady state or transient solver
- Conjugate heat transfer
- Boiling and cavitation models
- Extensive radiation capabilities
- Direct link to WAVE for time-step integration (co-simulation)
- Animation of results, plus export of pictures and movies for external use
- EnSight translator to allow for the viewing of Commercial CFD Solver results within CEI’s EnSight package

6.3 In-cylinder analysis

Commercial CFD Solver is used extensively in engine design because of its ease of use for moving boundary, in-cylinder applications. In-cylinder calculations can be performed to investigate various phenomena such as fuelling effects, spray injector positioning, piston shape and bowl design and the effects these have on combustion and emissions [43].

6.3.1 Key features

- Moving boundary and automatic meshing technique provides easy setup
  - Complex multi-cycle simulations can be performed with minimal user input
  - Rapid simulation turnaround allows maximum input to the design process
  - Discrete droplet modelling for sprays
  - Primary and secondary breakup models as well as droplet interaction
  - Extensive user function capability allows for modelling of user defined injector configurations
  - Internal injector flow to spray coupling
  - Extended spray set-up allows time and radial variation of injector/droplet characteristics
- Static and dynamic wall film capability
  - User function initialization and data extraction capability
- Auto-ignition and spark ignition models
  - Discrete particle ignition kernel model
- Commercial CFD Solver Two Zone Flamelet combustion model
  - Pre-mixed and non-premixed combustion
- Extensive internal validation programs and model development based on future engine technologies

6.4 Geometry and mesh setup

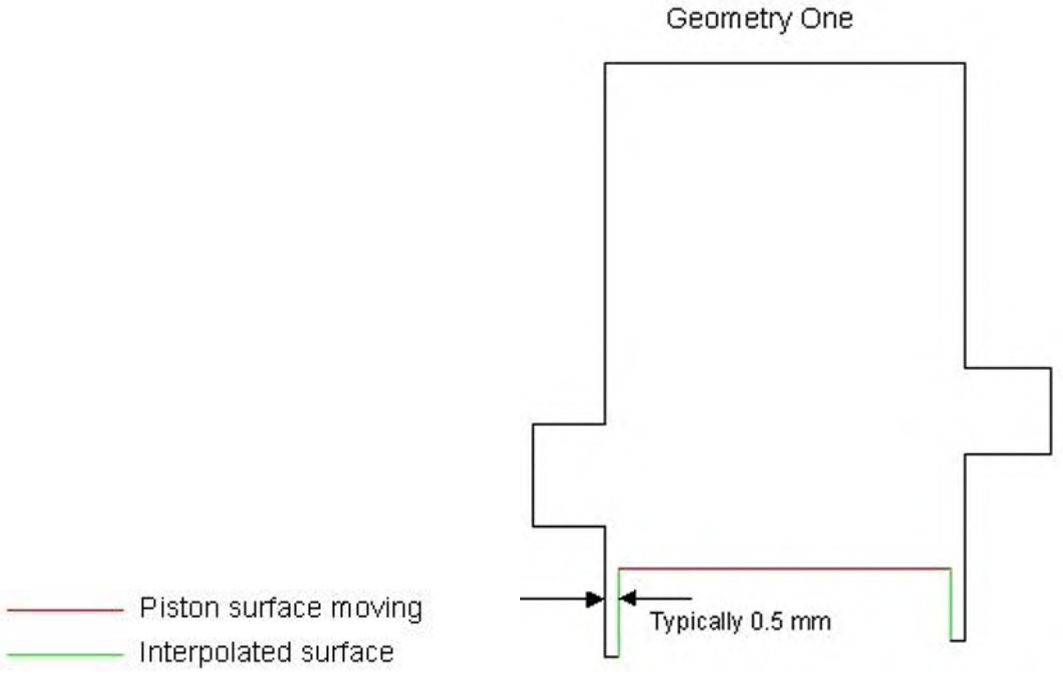

Fig. 6.1

The geometry shown in Fig. 6.1 is used to create the mesh files during the period when both the intake and exhaust ports are open. The small crevice around the piston is created by reducing the overall piston diameter slightly.

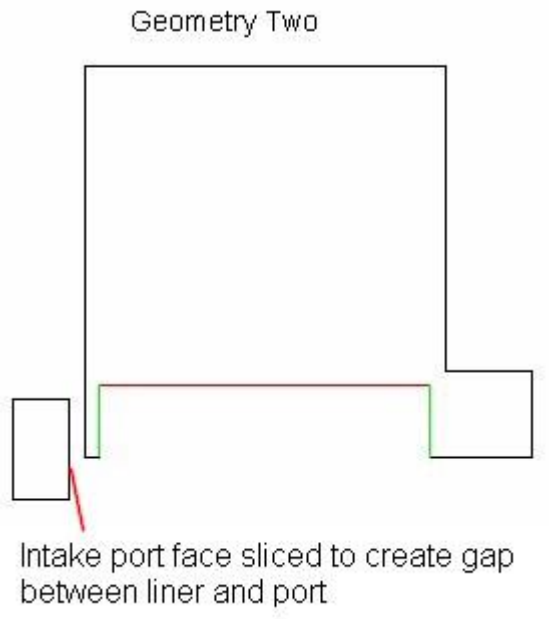

Fig. 6.2

The geometry shown in Fig. 6.2 is used to create the mesh files used during the period when only the exhaust port is open. The intake port is sliced such that there is a gap between the ports closed face and the liner.

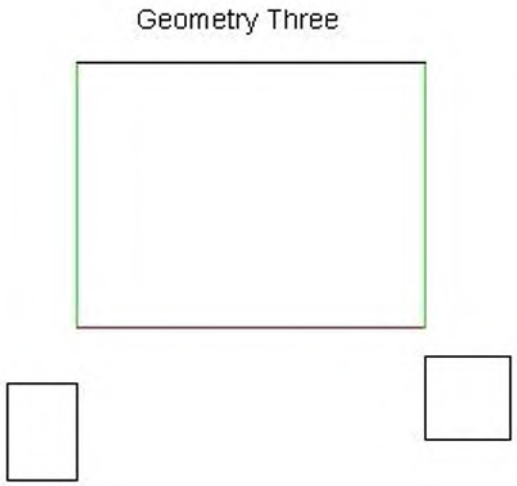

Fig. 6.3

The geometry shown in Fig. 6.3 is used to create the mesh files used when both the intake and exhaust ports are closed.

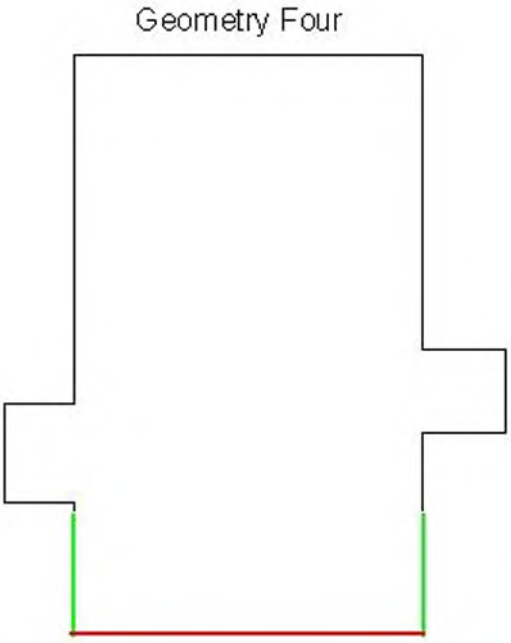

Fig. 6.4

The geometry shown in Fig. 6.4 is used when all the ports are open and the piston is below the all the ports. The crevice as in geometry one is not used here so that the mesh distortion etc is minimized.

The geometry used for this study is not based on a real engine and is a simple cylinder with 3 inlet ports and one exhaust port. The analysis is based on a motored 2 stroke engine cycle and so there is no fuel introduction or combustion included. Only the air motion and scavenging will be simulated.

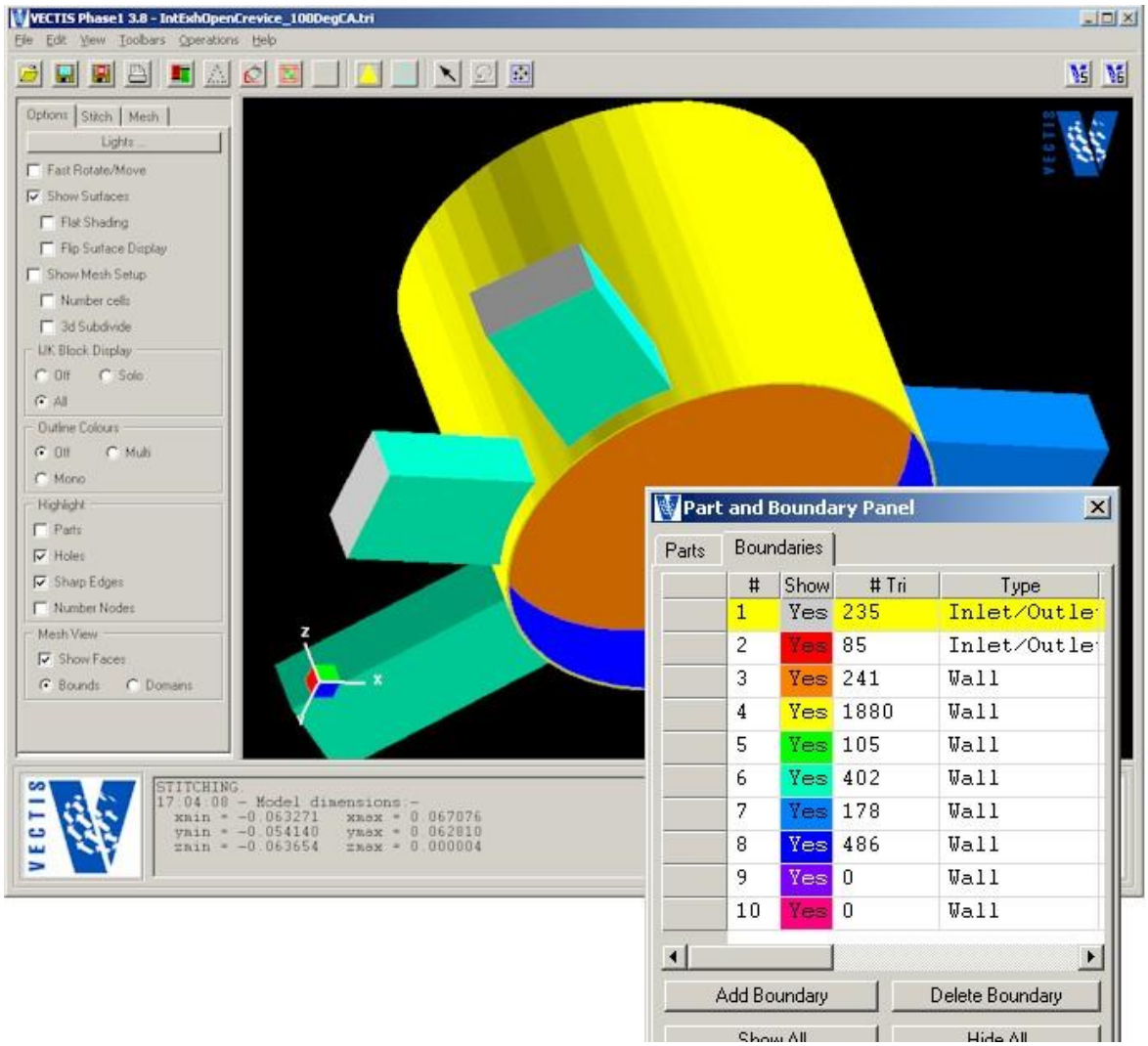

Fig. 6.5 Geometry and boundaries

Boundary Number	Surface
1	Inlet/Outlet boundary for intake ports
2	Inlet/Outlet boundary for exhaust port
3	Piston Surface
4	Stationary liner
5	Cylinder head surface
6	Intake port walls
7	Exhaust port wall
8	Interpolated Liner surface

The other three geometry files can be loaded and their boundary identification should be as shown above. As the geometry configuration is changed for the different files obviously there will be a change regarding which triangles belong to which boundary for the liner boundaries which are numbered 3 and 8.

As with all Commercial CFD Solver moving boundary calculations it is recommended that a run strategy is made at the start of the analysis preparation. The run strategy is used to identify at what crank angles the cross linking should occur and when the opening and closing events for the ports or valves (if included) will happen.

The run strategy for this analysis is shown below for the complete 360 degree 2 stroke cycle. The crank angles when a cross link will occur is shown, along with the geometry file to be used to create each mesh and also the timing for the port opening and closing events.

Port Open/Close Timings	
EPO	90
IPO	100
IPC	260
EPC	270

	Crank Angle	Motion	Mesh Position	Geometry File	Comments
1	0	F	0	Closed_	
2	15	F	15	Closed_	
3	30	F	30	Closed_	
4	45	F	45	Closed_	
5	60	F	60	Closed_	
6	75	F	75	Closed_	
7	82	F	82	Closed_	
8	89	F	89	ExhOpen_	Exhaust Ports Open
9	95	F	95	ExhOpen_	
10	100	F	100	IntExhOpenCrevice_	Intake Ports Open
11	105	F	105	IntExhOpenCrevice_	
12	110	F	110	IntExhOpenCrevice_	
13	115	F	115	IntExhOpenCrevice_	
14	118	F	118	IntExhOpenCrevice_	Bottom of Intake Port
15	120	F	120	IntExhOpen_	
16	135	F	135	IntExhOpen_	
17	150	F	150	IntExhOpen_	
18	165	F	165	IntExhOpen_	
19	180	F	180	IntExhOpen_	
20	210	F	210	IntExhOpen_	
21	220	F	220	IntExhOpen_	
22	224	F	224	IntExhOpen_	
23	228	F	228	IntExhOpen_	
24	240	F	240	IntExhOpenCrevice_	Bottom of Intake Port
25	247	F	247	IntExhOpenCrevice_	
26	252	F	252	IntExhOpenCrevice_	
27	256	F	256	IntExhOpenCrevice_	
28	260	F	260	IntExhOpenCrevice_	
29	265	F	265	ExhOpen_	Intake Ports Close
30	268	F	268	ExhOpen_	
31	270	F	270	ExhOpen_	
32	271	F	271	Closed_	Exhaust Port Closes
33	285	F	285	Closed_	
34	300	F	300	Closed_	
35	315	F	315	Closed_	
36	330	F	330	Closed_	
37	345	F	345	Closed_	
38	355	F	355	Closed_	
39	0	F	0	Closed_	

Table 6.1 Run strategy

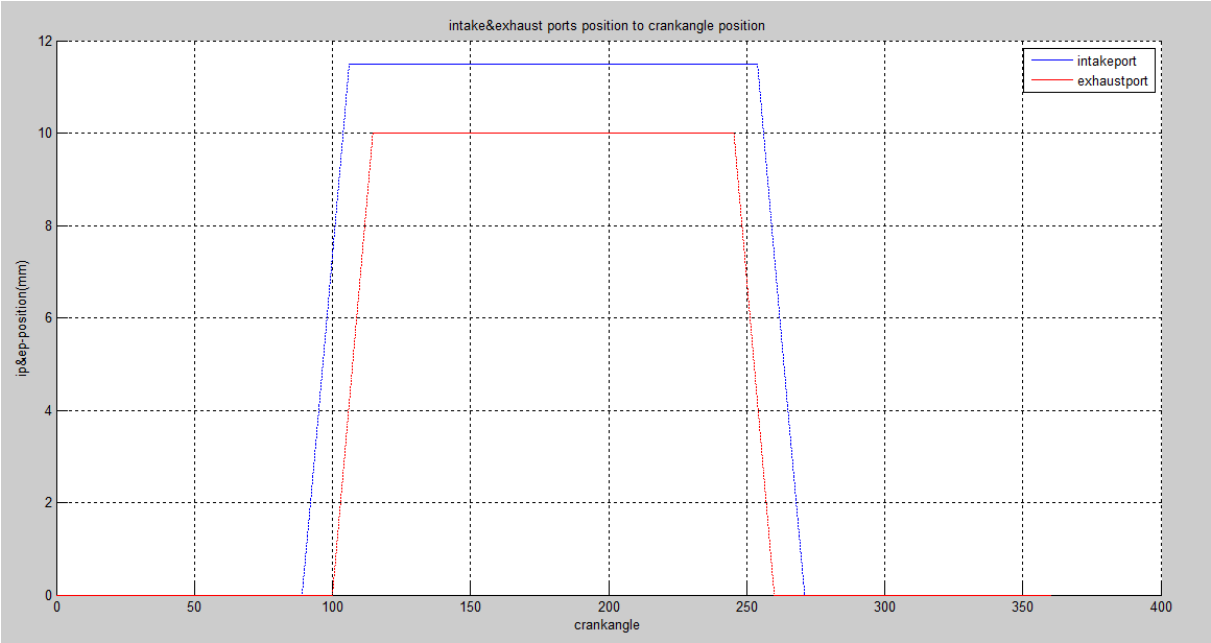

Fig. 6.6 Intake & exhaust ports positions

This run strategy can then be used with the Phase1 > Operations > Make Geometry function to create the geometry file required for each cross link.

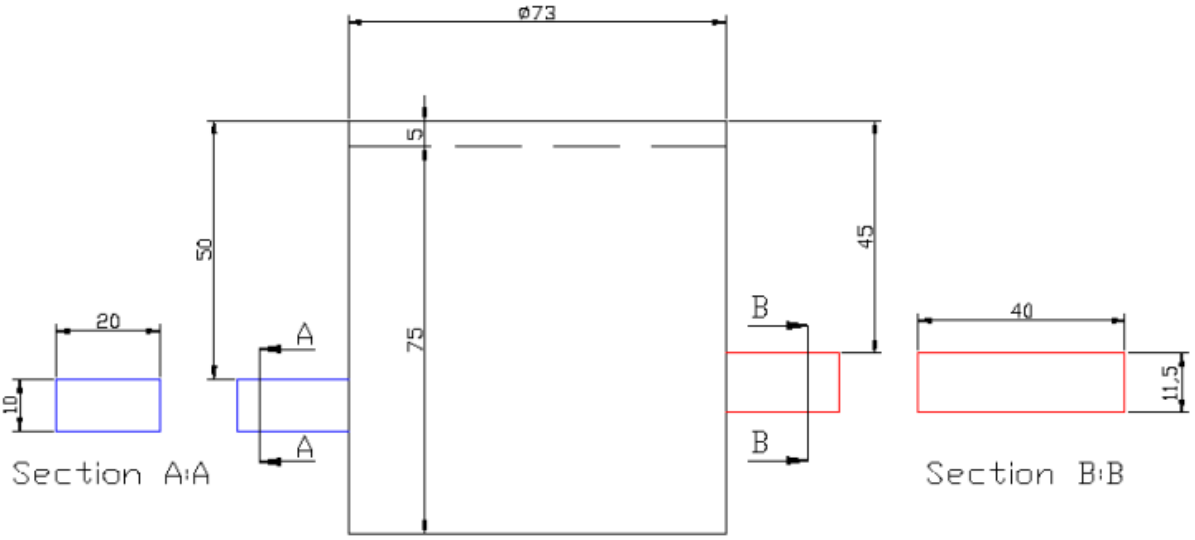

Fig. 6.7 Technical drawing of the geometry

Engine Specifications	
Bore	73 mm.
Stroke	75 mm.
Displacement	134 cc
Power	12 HP @ 4000 RPM
Torque	21.069 Nm.@ 4000 RPM

Table 6.2 Engine Specifications

7 Solver setup

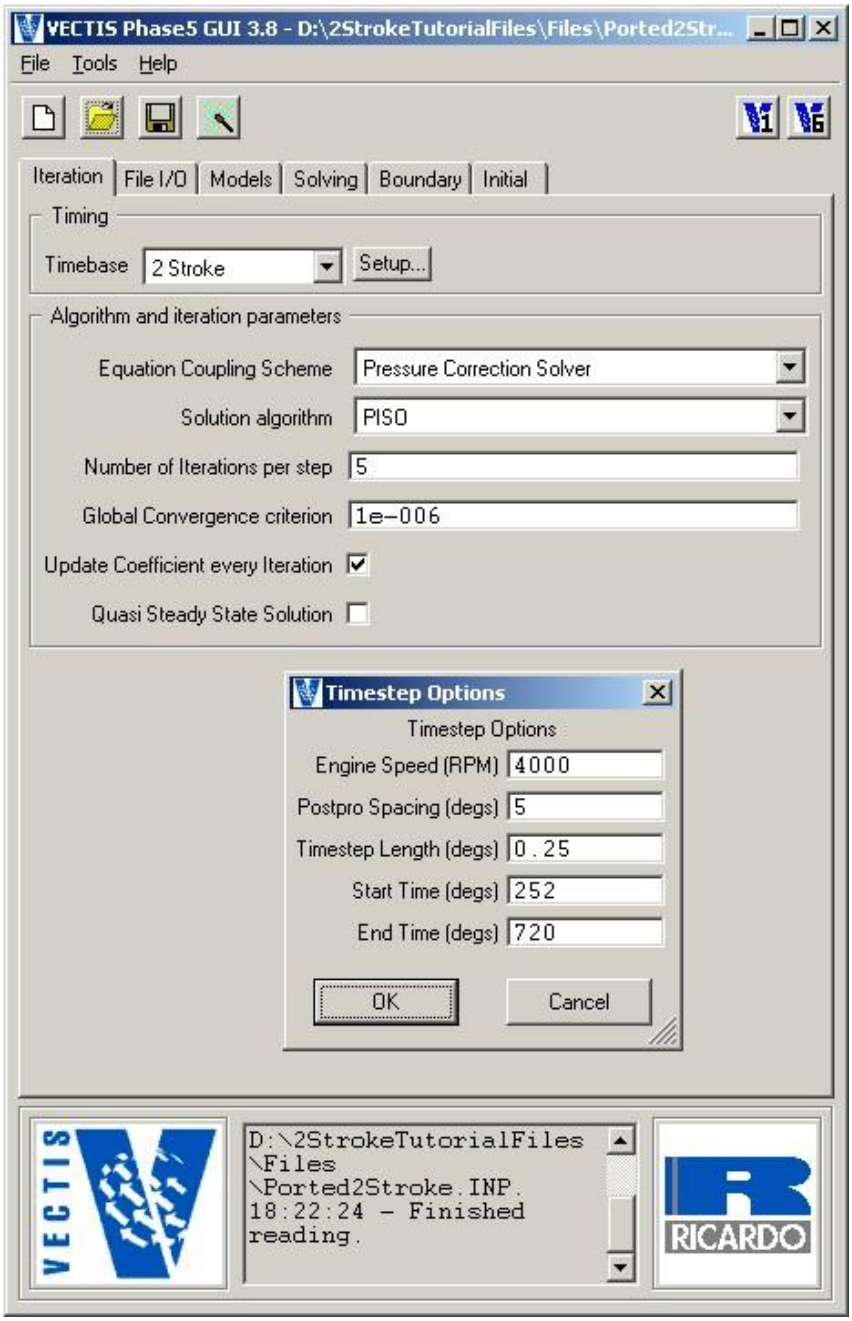

Fig. 7.1 Iteration panel

The Phase5gui > Iteration panel should show that the 2 stroke time base is being used so this means as is expected 1 cycle is from 0 to 360 degrees. All time dependent data is then defined based on this time base in crank angles.

The Timing > Setup panel shows an engine speed of 4000 RPM. The post processing spacing is 5 degrees which should ensure that the POST file contains frequent time entries whilst the file size does not become too large. A time step of 0.25 degrees crank angle is being used which is usually acceptable for the air motion only analysis. If combustion is included or the analysis experiences stability issues then this could be reduced. Typically for combustion 0.03125 or 0.015625 degrees CA should be used.

The start time is set to be 252 degrees which is near the intake port close position. The end time is set to 720 degrees. Therefore the analysis will calculate the flow solution for the last 108 degrees of the first cycle (252 to 360 degrees CA) and then the complete 360 degrees (360 to 720 degrees CA) of the second cycle.

The reason for this start time is that the first 108 degrees will allow the in cylinder and port flow fields to initialize before the 2nd cycle starts. This should then make the second cycle more accurate since the flow field will have a better cyclic representation.

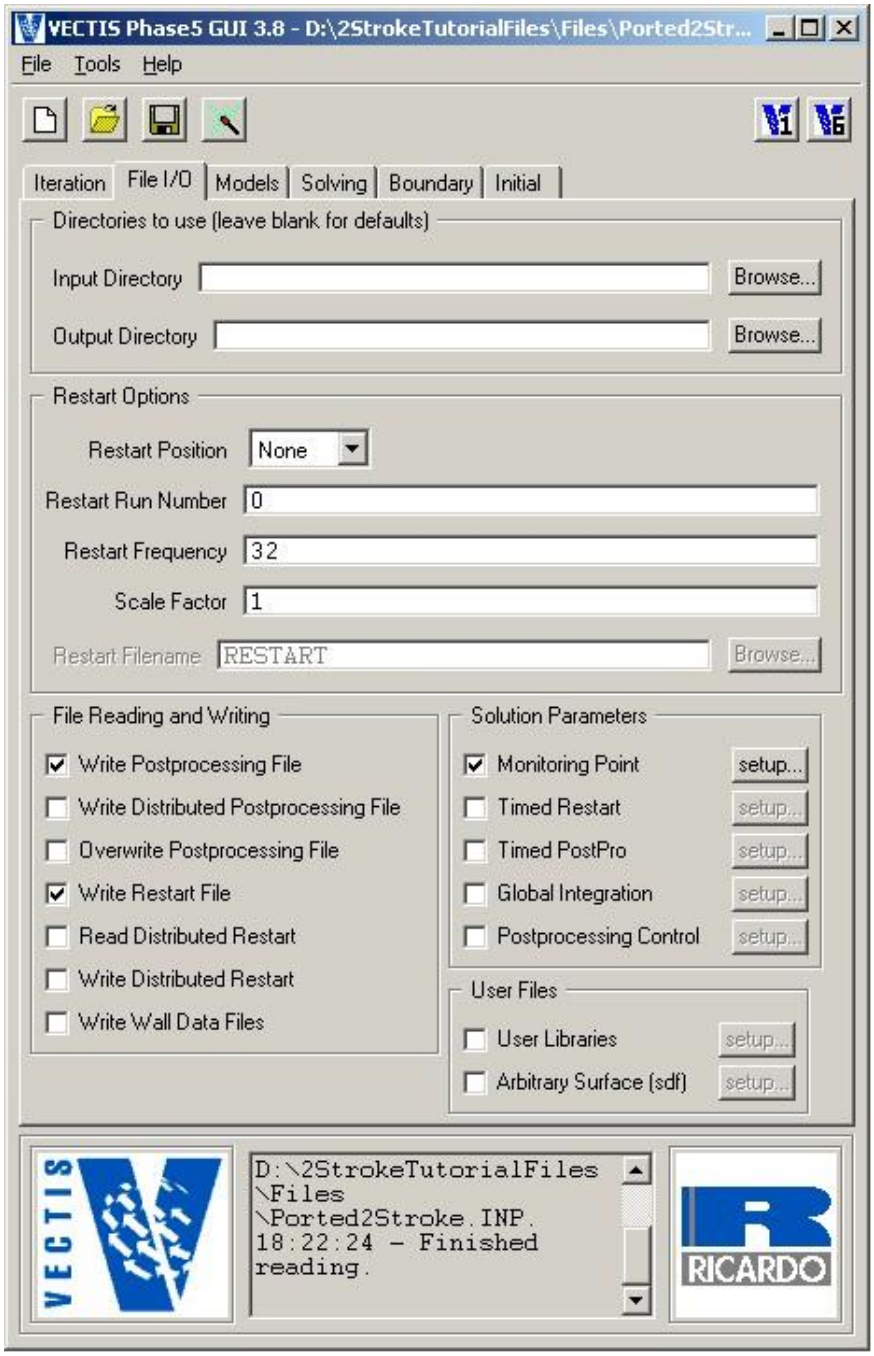

Fig. 7.2 File IO panel

The Phase5gui > File IO panel as shown below is used to define the restart frequency as 32 time steps. Since the time step has been defined as 0.25 degrees CA this means the RST1 and

RST2 files will be created every 8 degrees CA. This setting is always a compromise between time lost as the solver writes to the disk against lost time if the analysis stops due to a hardware issue of stability problem.

The write post processing and restart file options are selected. Also three monitoring points have been setup in the central inlet port, chamber and exhaust port. They have been set up using real space XYZ co-ordinates so that if the mesh setup is changed they are still valid.

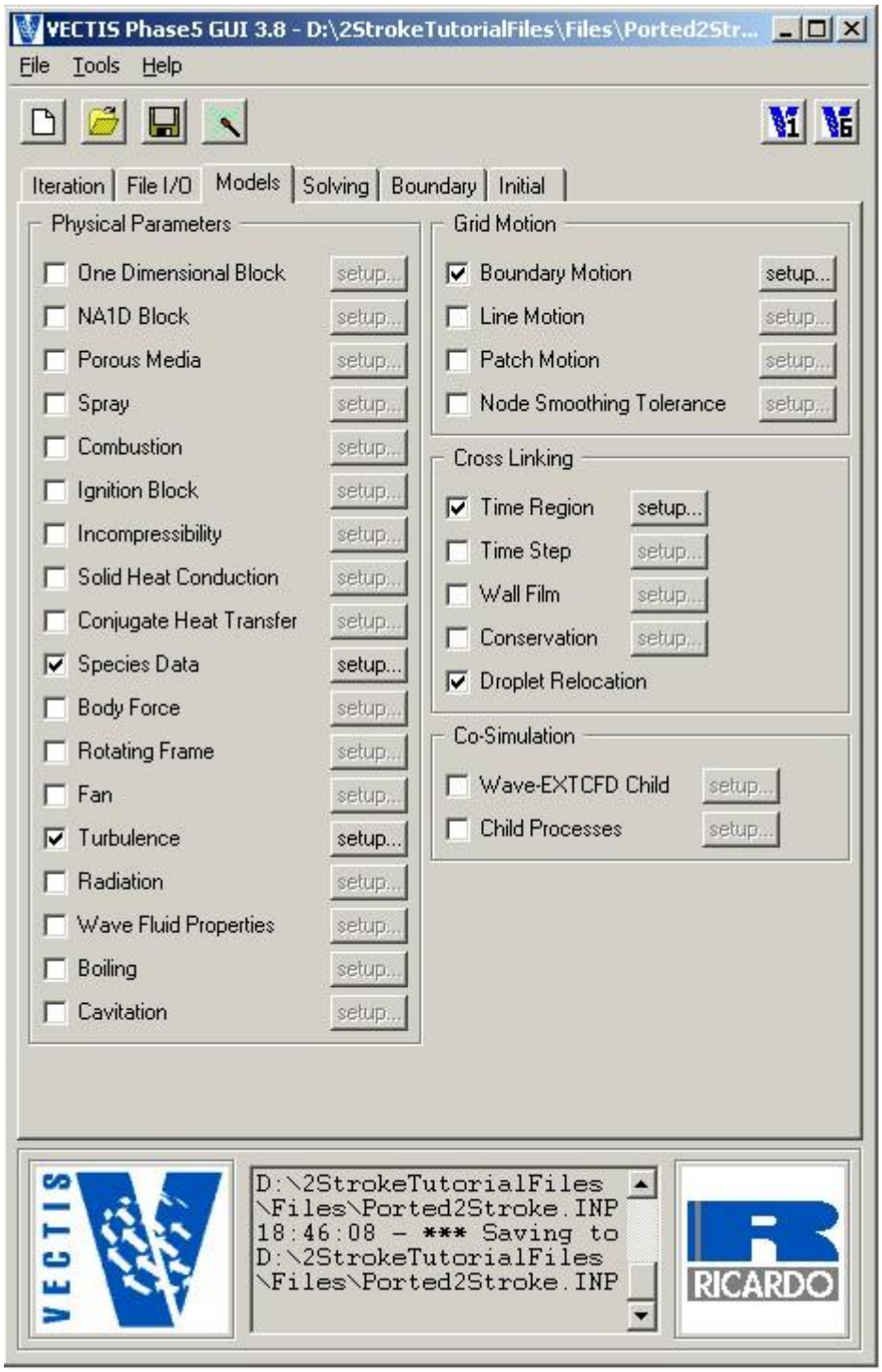

Fig. 7.3 Models panel

The Phase5gui > Models panel is shown below. The species and turbulence are left as default i.e. species order is the Commercial CFD Solver standard order and is Fuel, Air, Products and Inerts.

The time region panel is used to define the cross linking strategy which is determined from the run strategy table shown above.

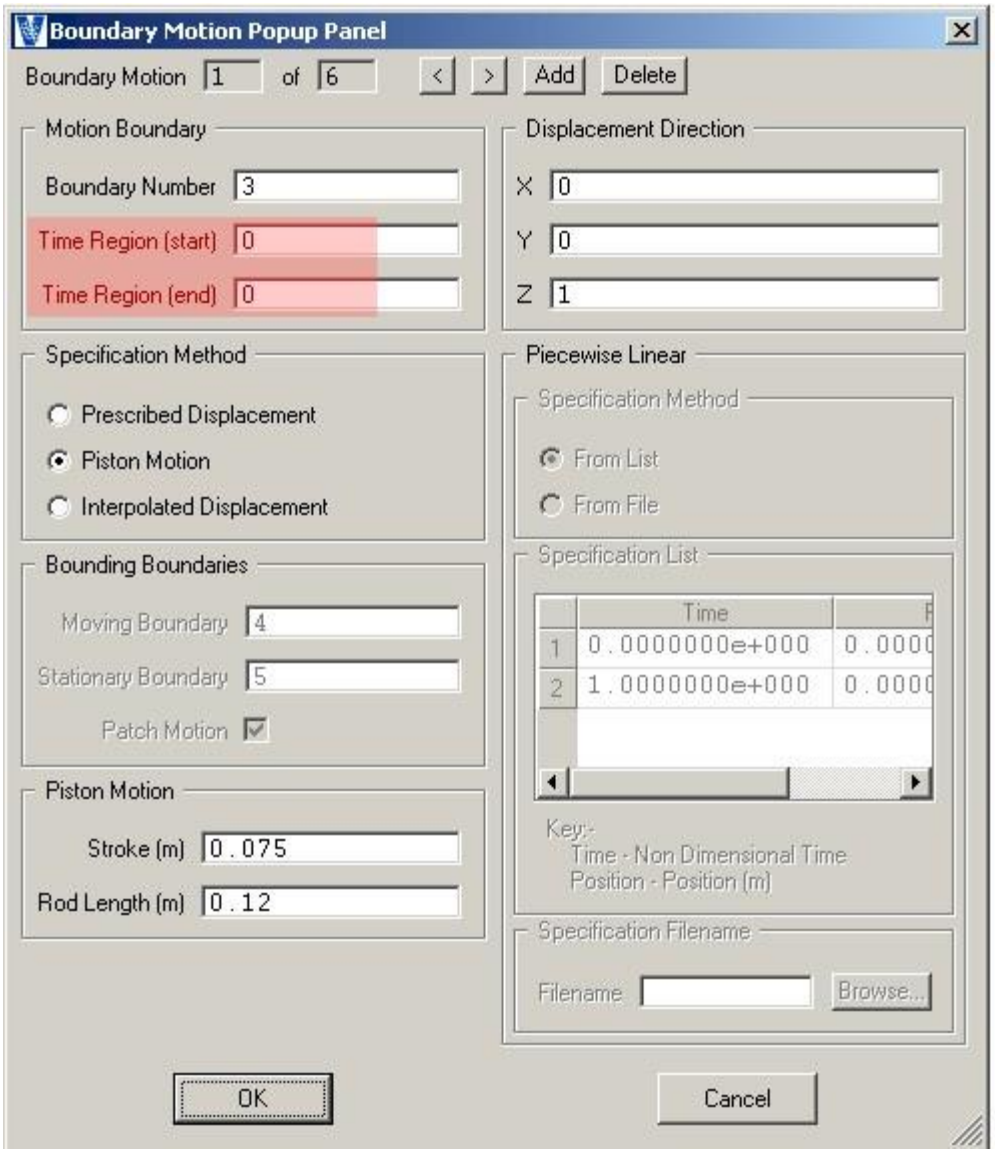

Fig. 7.4 Boundary motion panel 1

An important point to note with Commercial CFD Solver ported 2 stroke engine analyses is that different time regions i.e. meshes will have different boundary motion setup information. This is mainly due to the crevice configuration and as a consequence the vector directions between the moving piston and stationary wall changing.

The first boundary motion panel as shown below is for the piston surface and this is set to have both the first and last time region as 0. This means that this boundary motion specification will apply for the whole engine cycle.

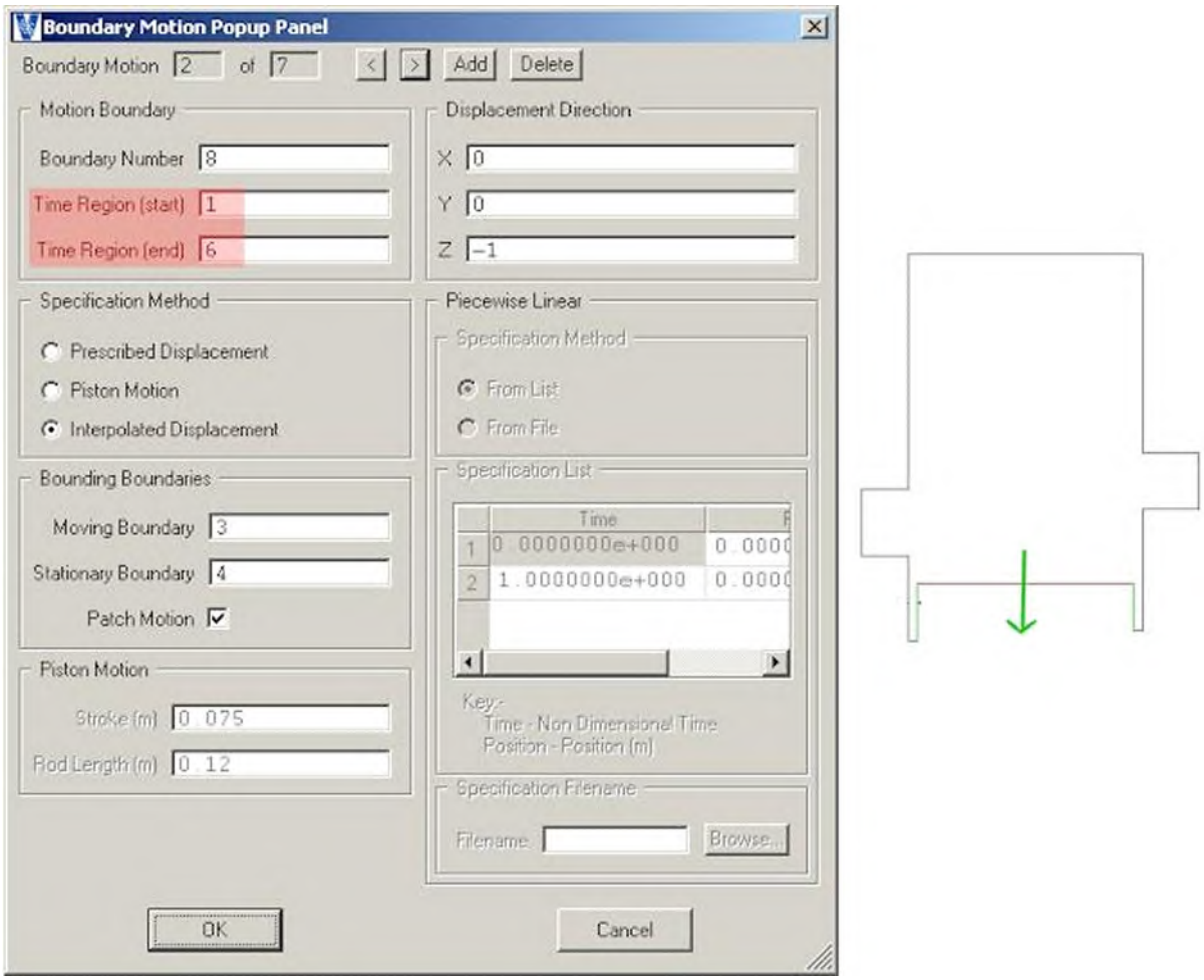

Fig. 7.5 Boundary motion panel 2

The second boundary motion entry is for the interpolated liner surface during time regions 1 to 6. During these time regions the mesh files being used are 252.DAT to 270.DAT and they include the crevice geometry so this means the vector from the moving piston to the stationary surface is 0 0 -1 as shown Fig. 7.5. This can be confirmed by referring to the run strategy above.

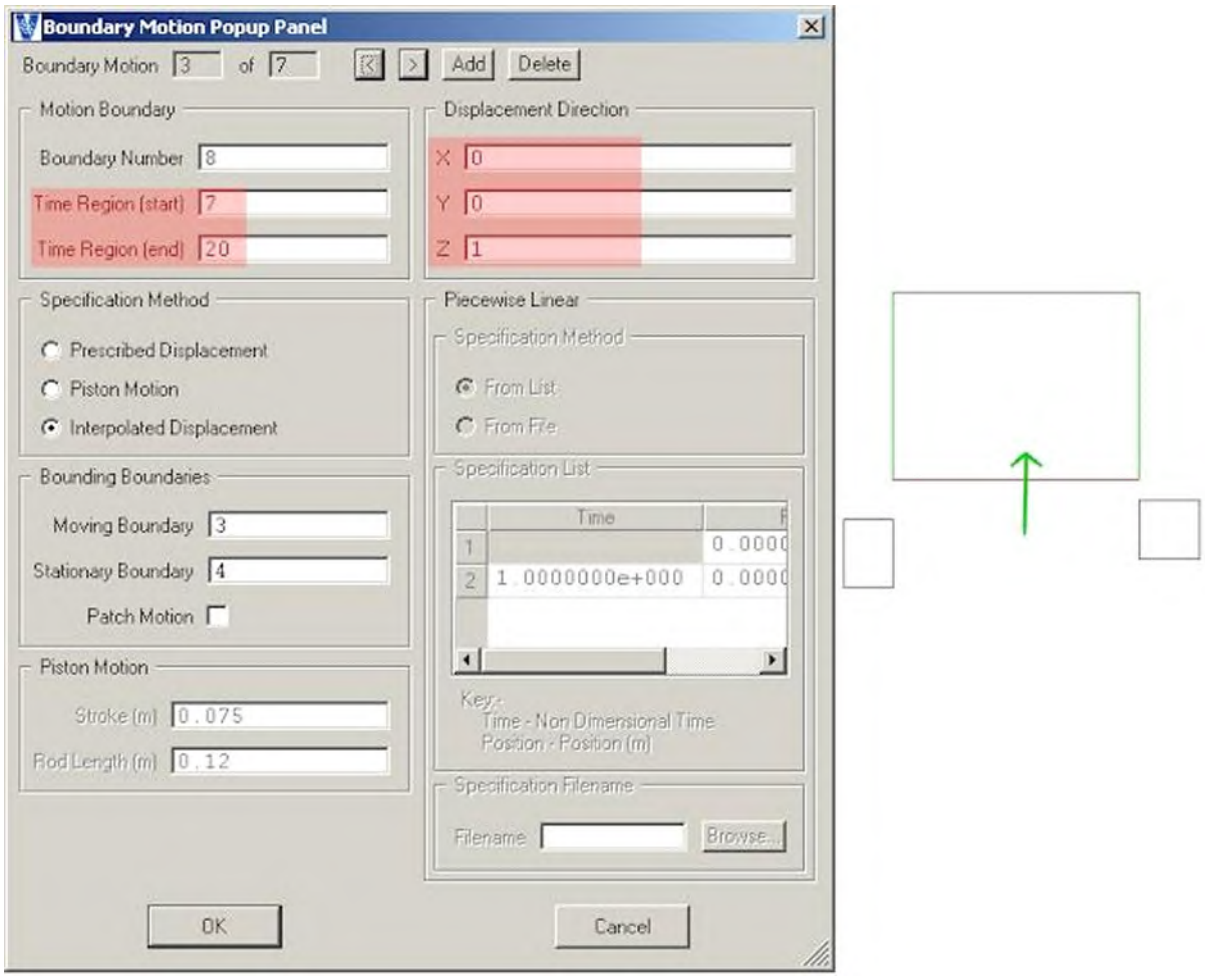

Fig. 7.6 Boundary motion panel 3

The third boundary motion specification is again for the interpolated liner surface and is defined for time regions 7 to 20. This is for mesh files 271.DAT to 082.DAT. These mesh files do NOT include the crevice geometry and so now the vector from the moving piston surface to the stationary cylinder head surface is 0 0 1 as shown below.

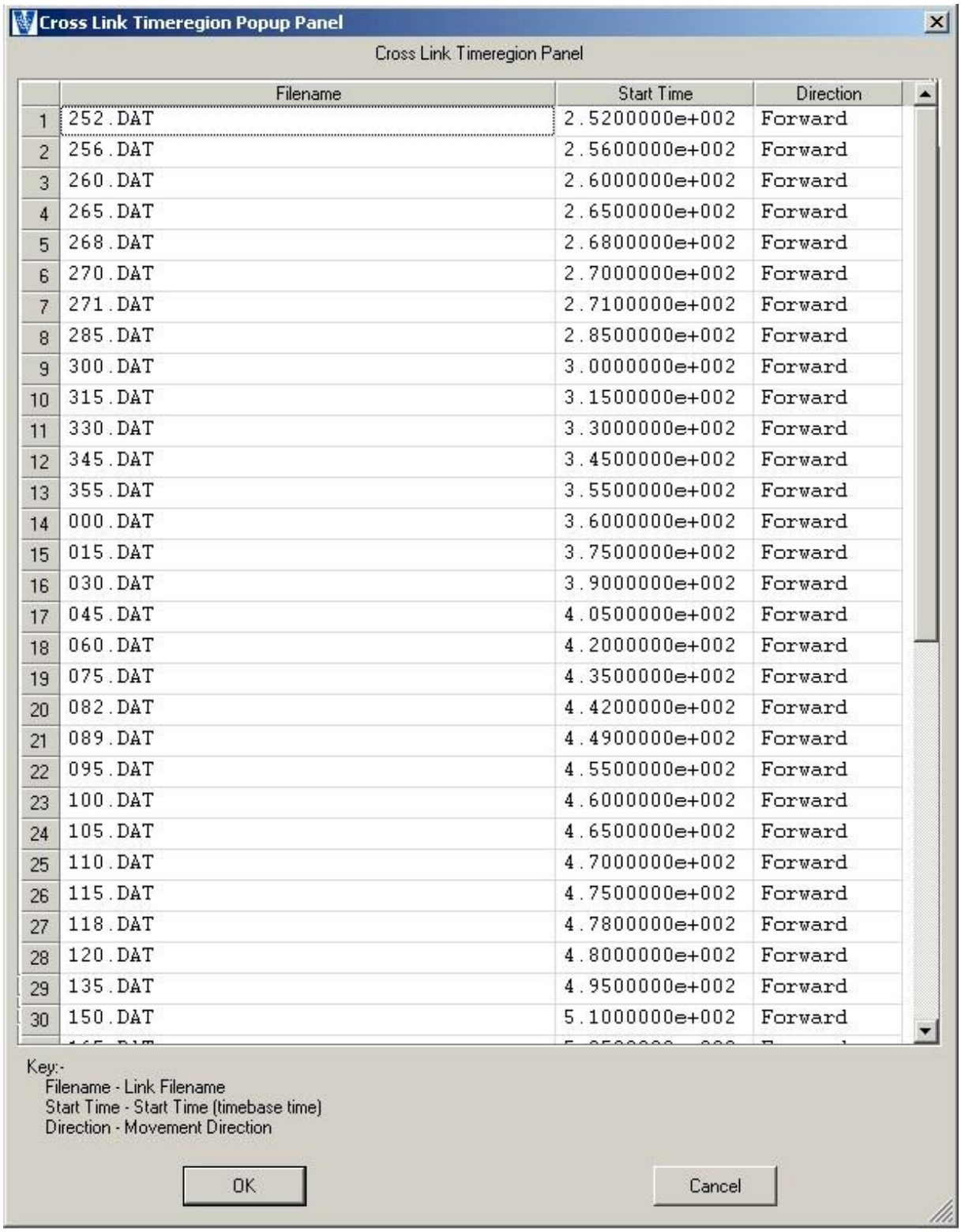

Fig. 7.7 Time region panel

The boundary motion specification 4 to 7 follows this setup method.

The Phase5gui > Models > Time Region panel is used to define at what time a cross link should occur and which mesh should be loaded. Each mesh represents a time region as show in Fig. 7.7.

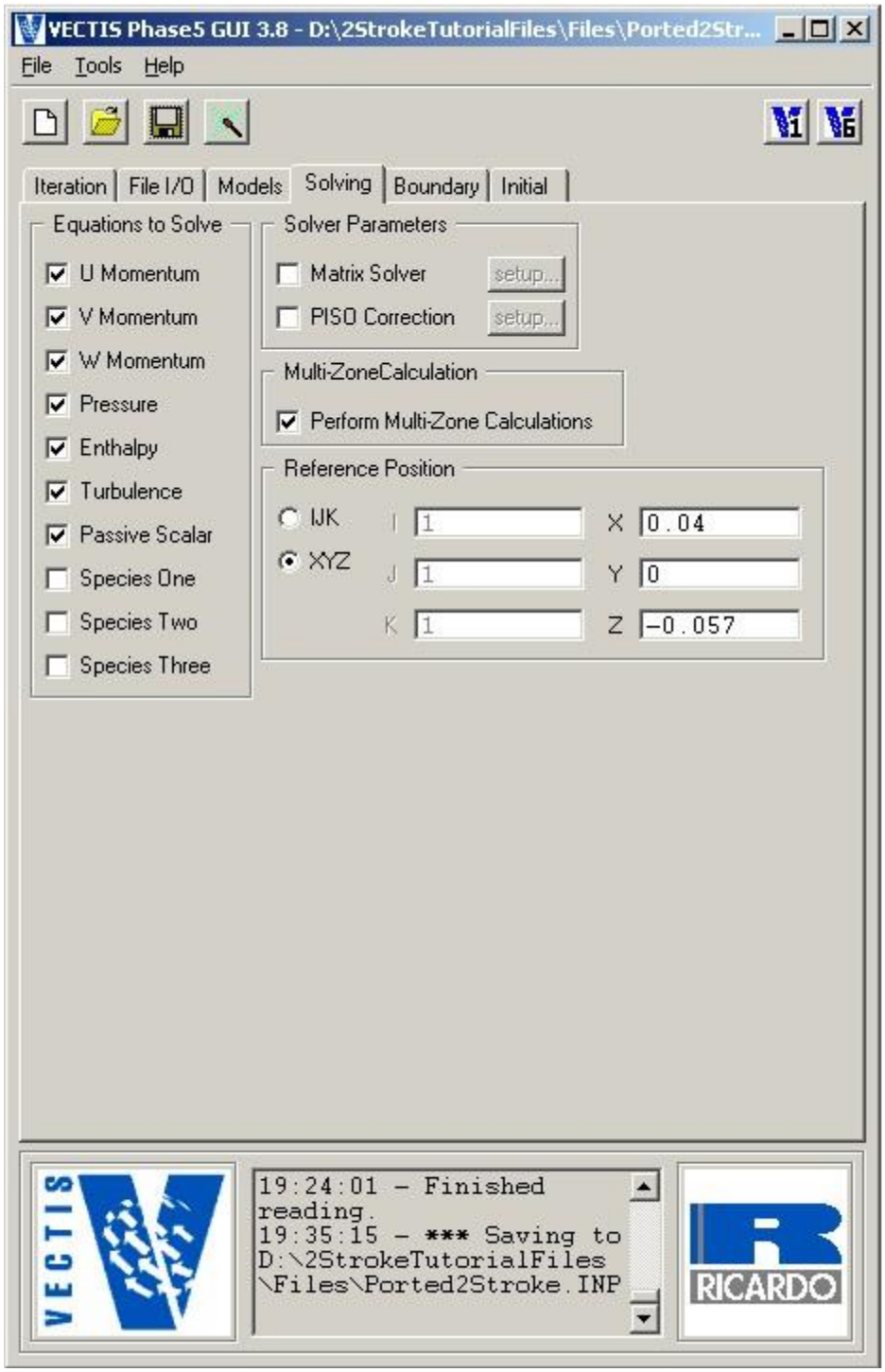

Fig. 7.7 Solving panel

The phase5gui solving panel is used to turn on the required equations and define a reference pressure location. For this analysis all the equations are turned on except the species equations since the working fluid will be air only so there is no need to solve any species transport equations.

The reference pressure position has been entered using XYZ co-ordinates for a location in the exhaust port. Since the pressure correction solving scheme are used (defined in the Iteration

panel) the reference pressure will be set equal to the initial pressure (to be defined in the Initial panel) at the defined reference pressure position.

Also the Perform multi zone option has been turned on.

Fig. 7.8 Boundary panel

The boundary panel is fairly self-explanatory for this analysis in that there are two inlet/outlet boundaries defined in the Inlet/Outlet panel. Each boundary then has an associated Zero Dimensional data set used to define a Total pressure inlet boundary for the intake ports with

pressure 1.1 bar and a static pressure outlet boundary for the exhaust port with a pressure of 1 bar.

Each wall boundary is set as a constant 300 Kelvin's temperature surface.

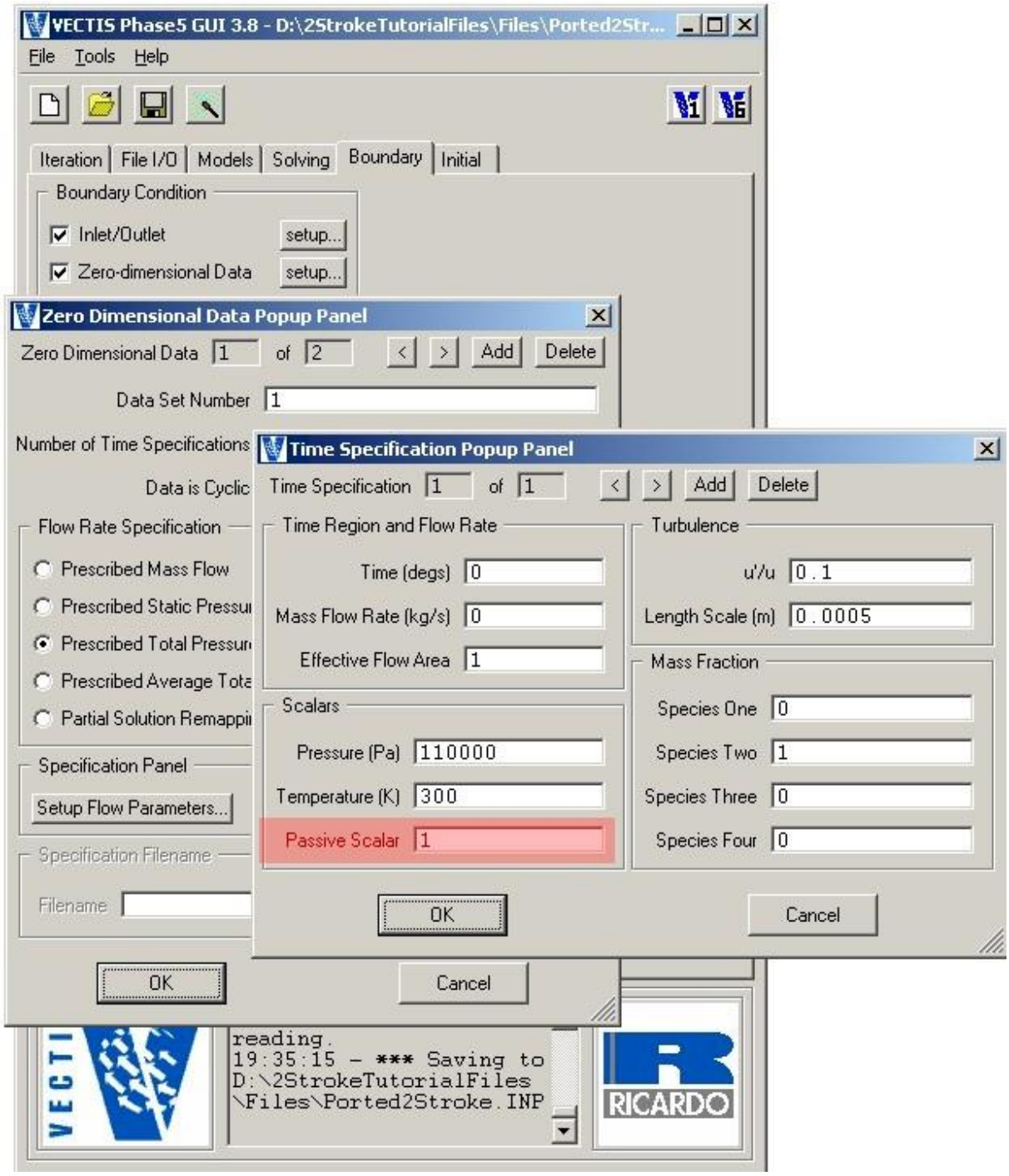

Fig. 7.9 Zero dimensional data panel

One important detail concerning the zero dimensional data set for the intake port IO boundaries is that the passive scalar fraction is set to 1 i.e. 100%. This will then allow the passive scalar distribution to be used to give an idea of the scavenging efficiency of the 2

stroke engine. If the passive scalar is required the passive scalar equation must also be turned on in the phase5gui solving panel.

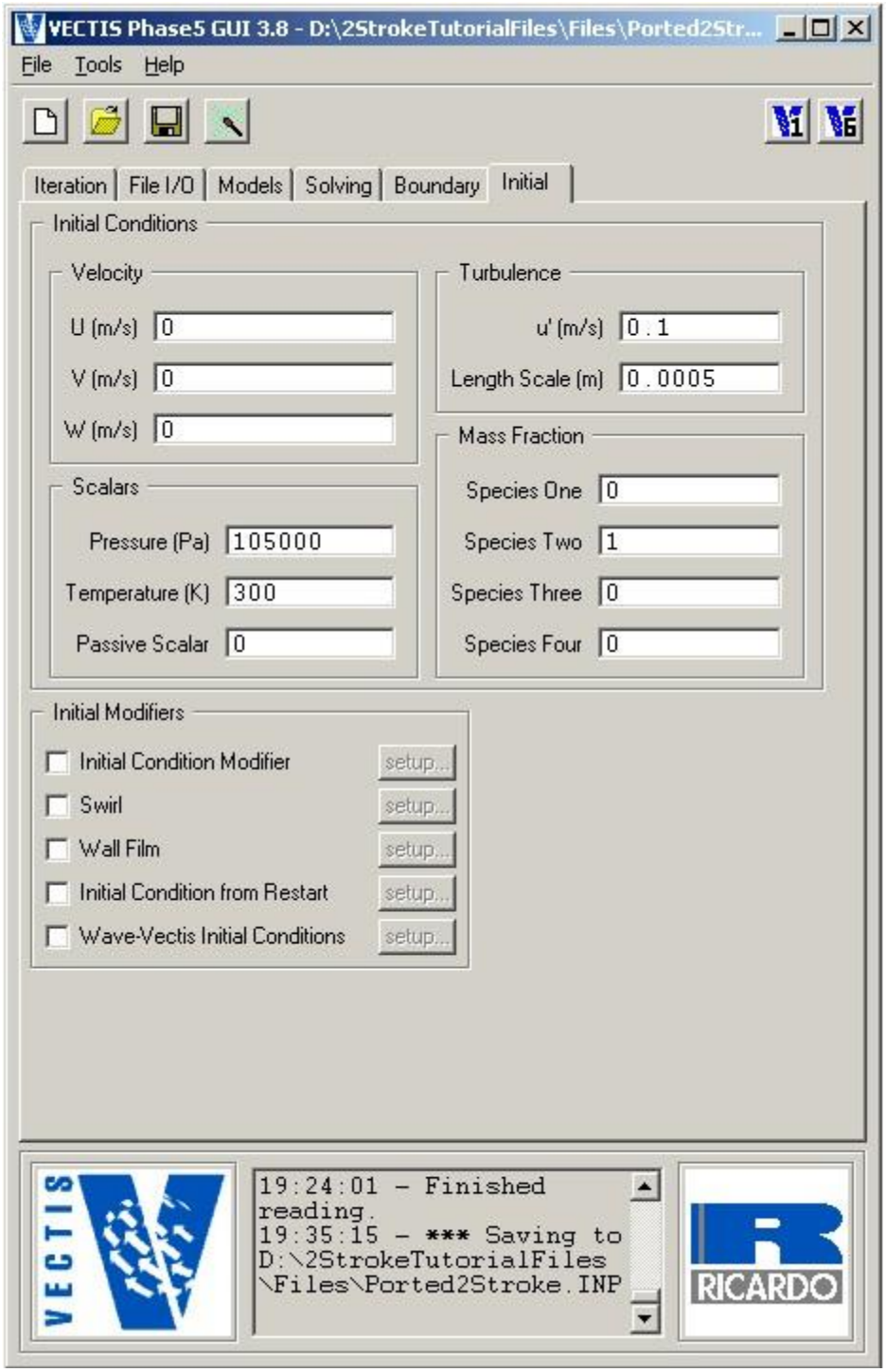

Fig. 7.10 Initial panel

The phase5gui initial panel as shown below is used to define the global initial conditions as 1.05 bar and 300 Kelvin's. The pressure is chosen to be half way between the boundary pressures. There are no initial condition modifier blocks set up since this analysis is only using air as the working fluid. If combustion was included then initial condition modifier blocks can be used to define the initial air, fuel and residuals distribution.

The solver input file setup detail has now been covered and the calculation can now be started.

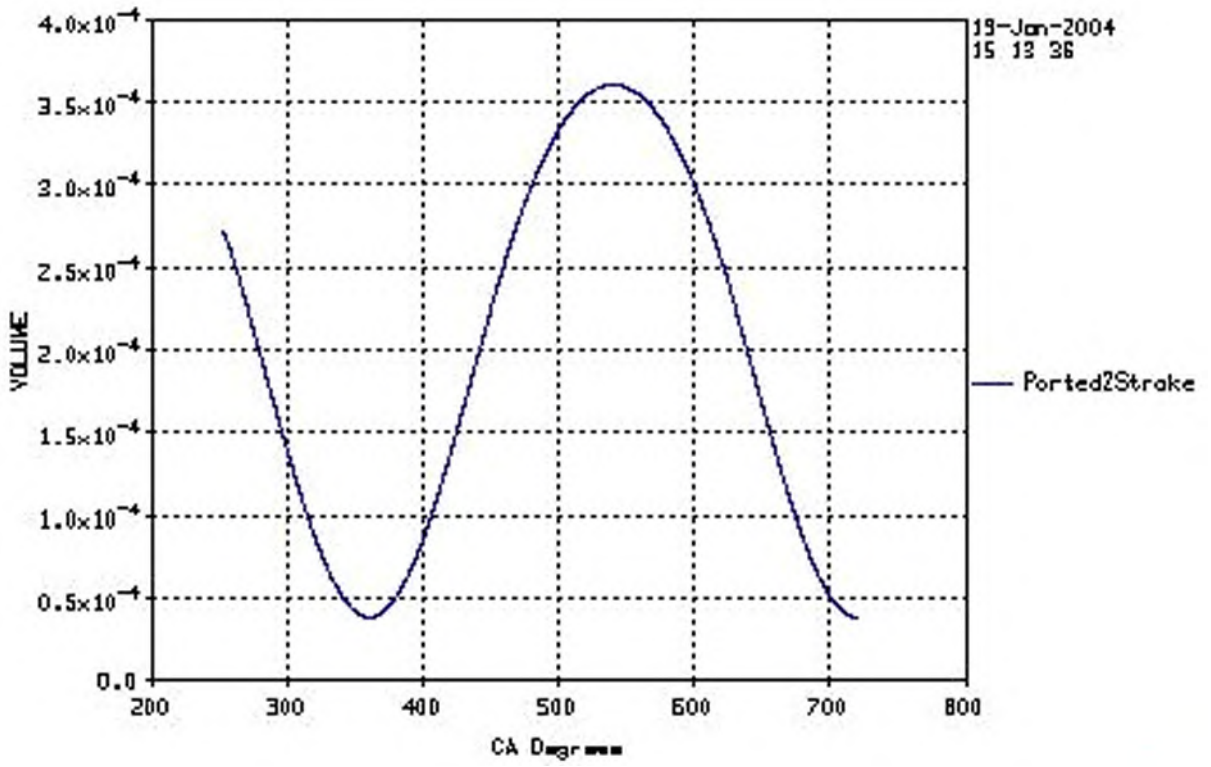

Fig. 7.11 Volume-Crank angle degree

8 Solution results

8.1 Total pressure

In physics, the term total pressure may indicate two different quantities, both having the dimensions of a pressure:

- In fluid dynamics, total pressure (p_0) refers to the sum of static pressure p, dynamic pressure q, and gravitational head, as expressed by Bernoulli's principle:
  $P_0 = p + q + \rho g z$
  where ρ is the density of the fluid, g is the local acceleration due to gravity, and z is the height above a datum.
  If the variation in height above the datum is zero, or so small it can be ignored, the above equation reduces to the following simplified form: $P_0 = p + q$

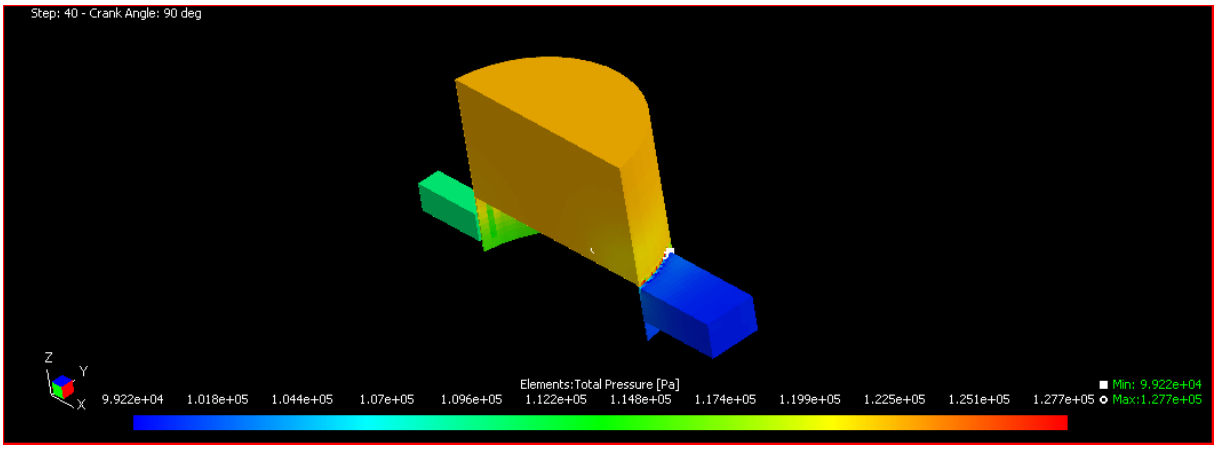

Fig. 8.1 Total pressure disturbance when the exhaust port opening

In Fig. 8.1, you can see clearly intake ports' pressure higher than the exhaust port's pressure. You know, air coming from the intake ports and when the intake ports closes there will be a pressure higher than the atmospheric pressure. However, in the exhaust port, it is opened to outside.

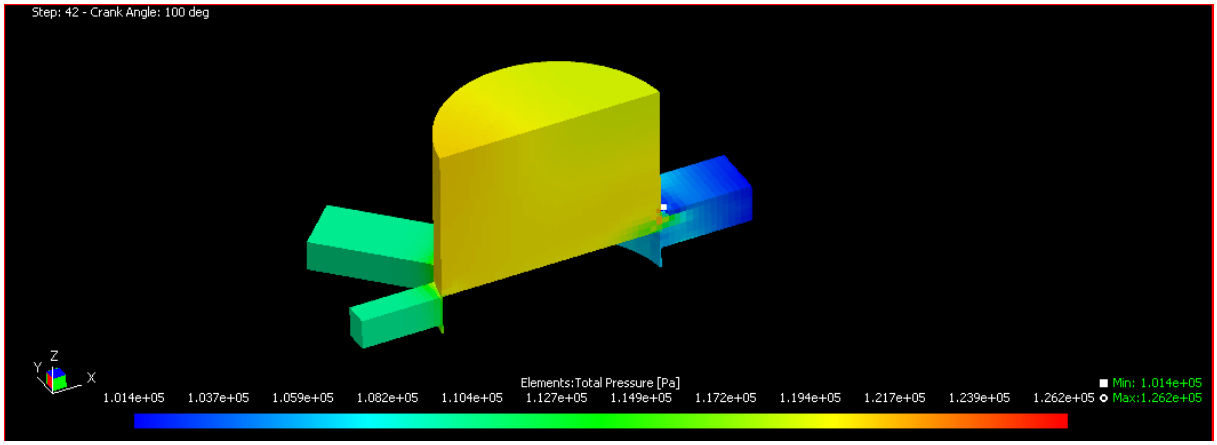

Fig. 8.2 Total pressure disturbance when the intake ports opening

In Fig. 8.2, there is a low pressure area in the exhaust port. Because, in the exhaust port, there is a flow starts.

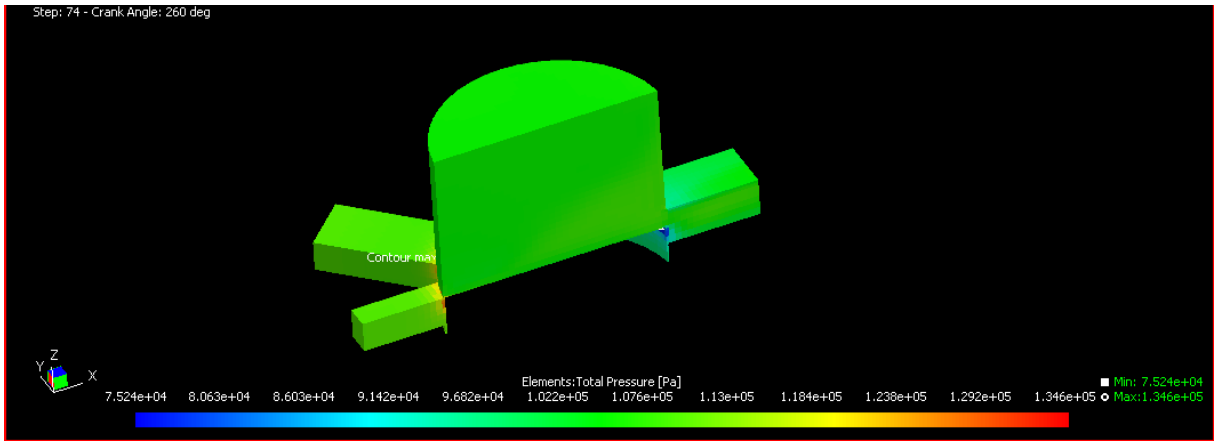

Fig. 8.3 Total pressure disturbance when the intake ports closing

In Fig. 8.3, intake ports are closed, so there will occur a max. pressure point.

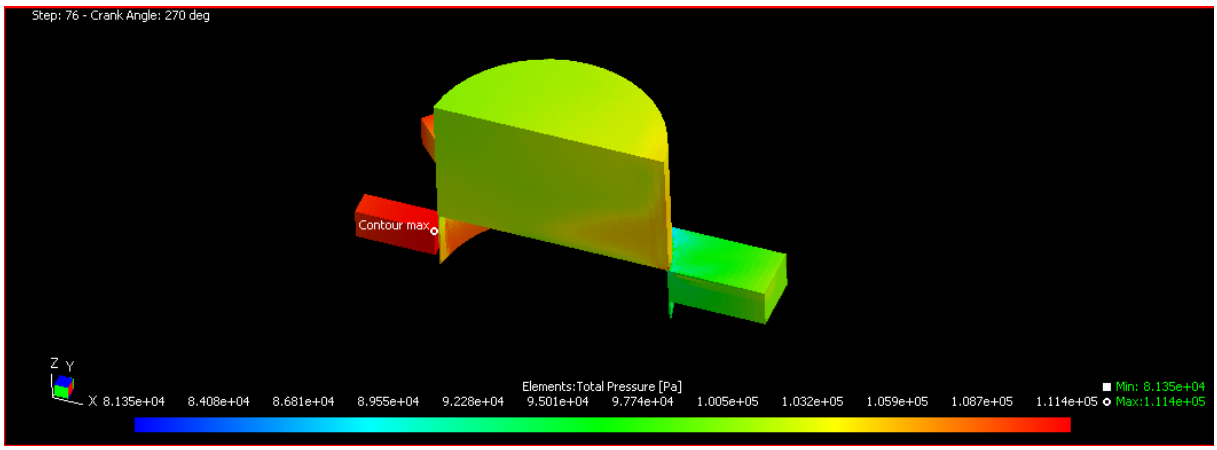

Fig. 8.4 Total pressure disturbance when the exhaust port closing

In Fig. 8.4, after intake ports closing, the pressure will increase in the intake port. This became, because flow in the intake ports will be stopped actually.

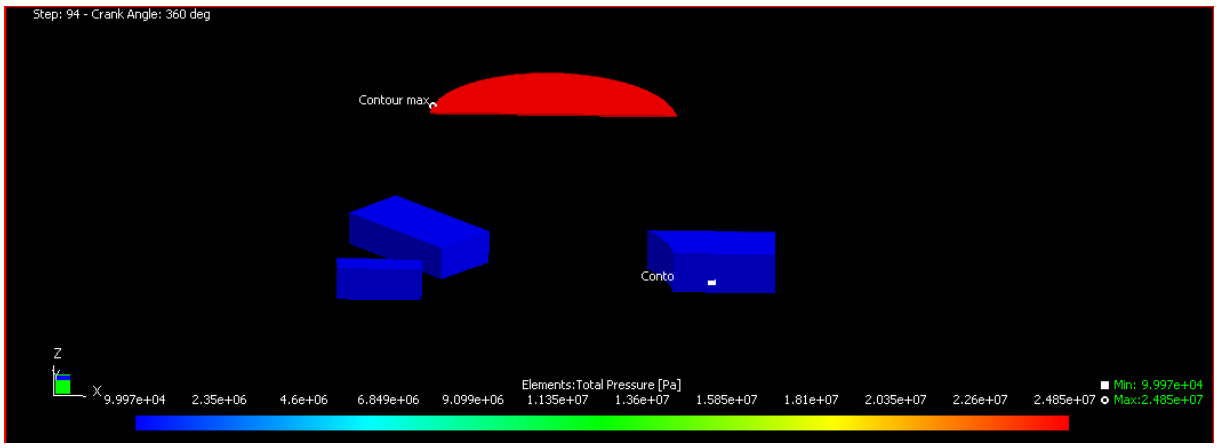

Fig. 8.5 Total pressure disturbance at the TDC

In Fig. 8.5, you can see clearly the pressure disturbance at the TDC. This state is the point that the system reaches the maximum pressure. This situation becomes at the 360 degrees crank

angle position. When this time, max. pressure is 24.85 Mpa. This is the pressure that the motor torque is got.

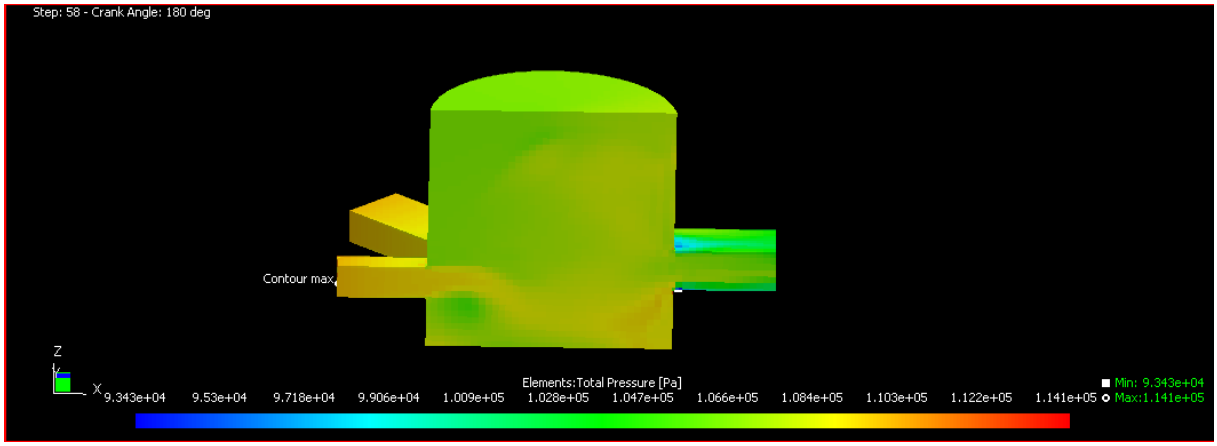

Fig. 8.6 Total pressure disturbance at the BDC

In Fig. 7.6, you can see the total pressure disturbance at the BDC. In this position, max. pressure occur at the inlet port. That is an understandable situation for two-stroke engine, because on this position intake and exhaust ports both open. So from crank turning, there will be some pressure to the in cylinder. This occur flow in to the cylinder and out of the cylinder.

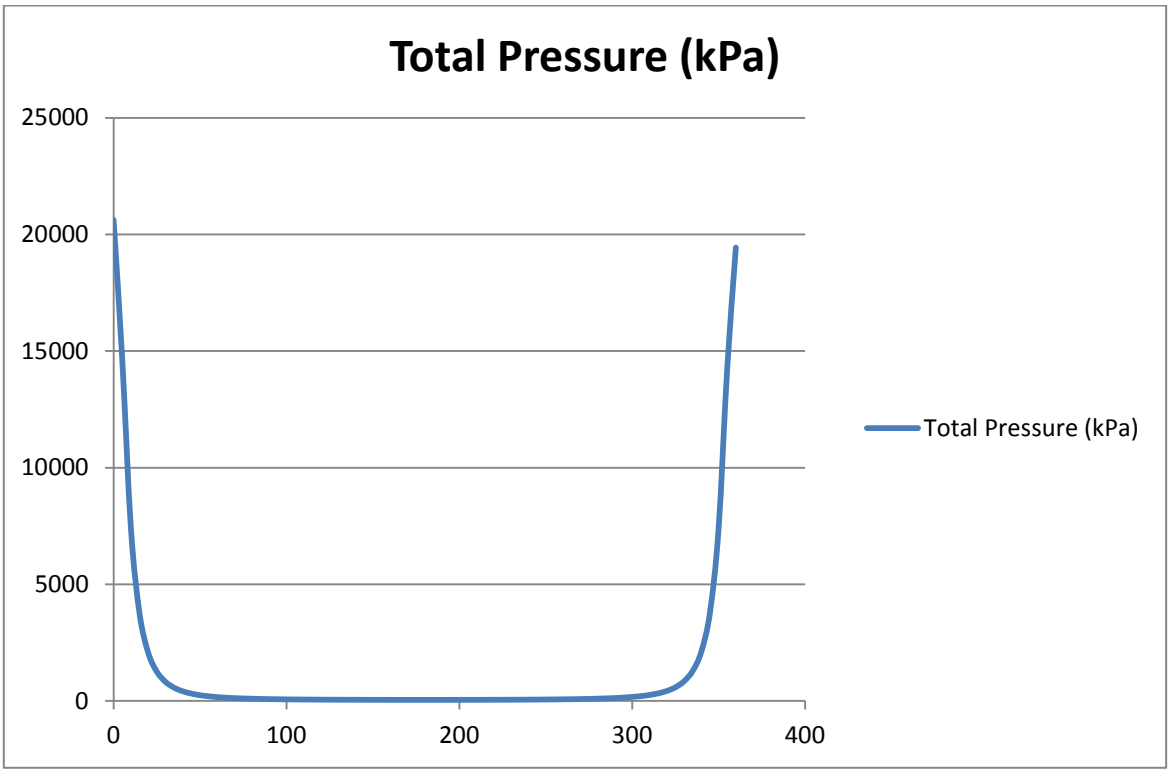

Fig. 8.7 Total pressure values to crank angle

8.2 Temperature

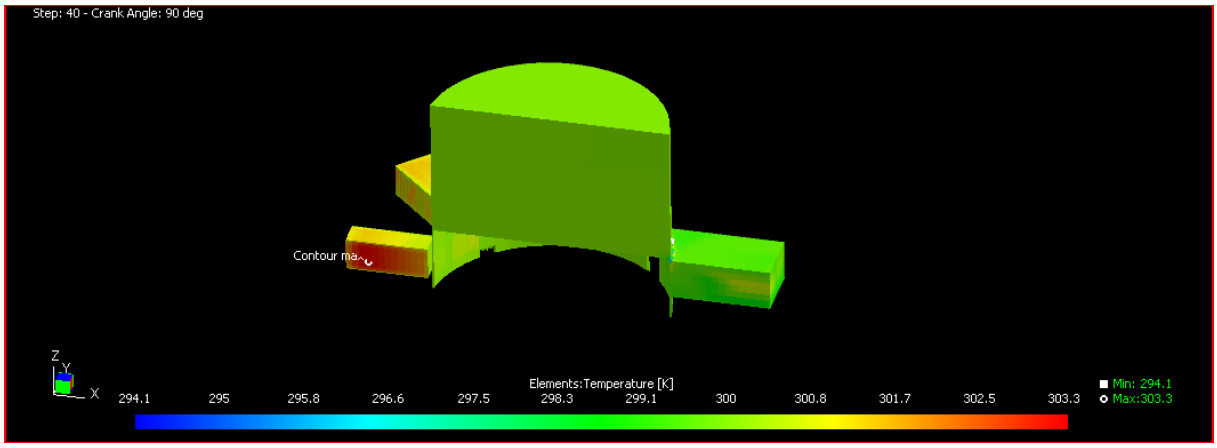

Fig. 8.8 Temperature disturbance when the exhaust ports opening

In Fig. 8.8, you can see the max temperature at this crank angle at the inlet ports. This is easy to understand, because in the Fig. 8.1, you can see max. pressure will occur at the inlet port at this crank angle.

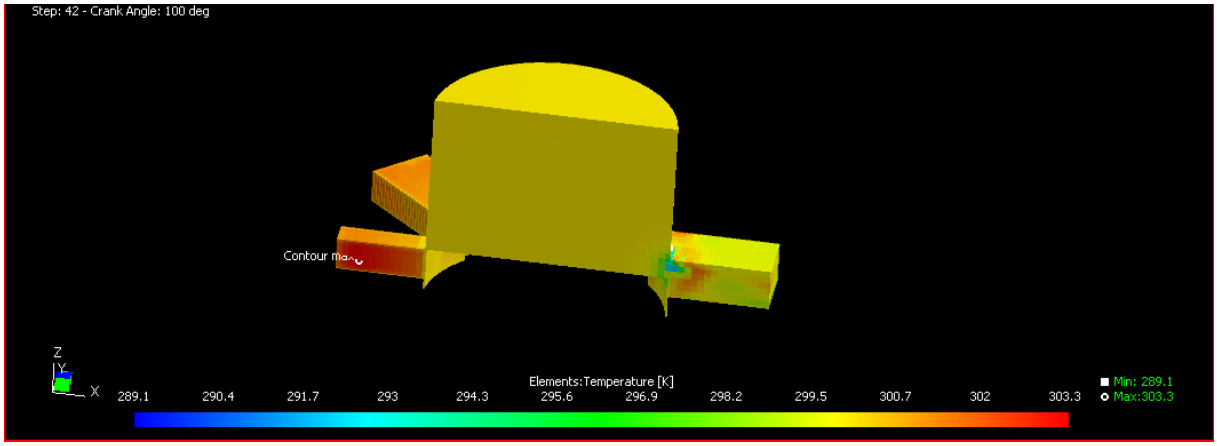

Fig. 8.9 Temperature disturbance when the intake ports opening

In Fig. 8.9, the min. temperature occurs at the exhaust port. Because, the flow started at the exhaust port 10 crank angles before. If there is a flow, pressure and temperature decreases at this location.

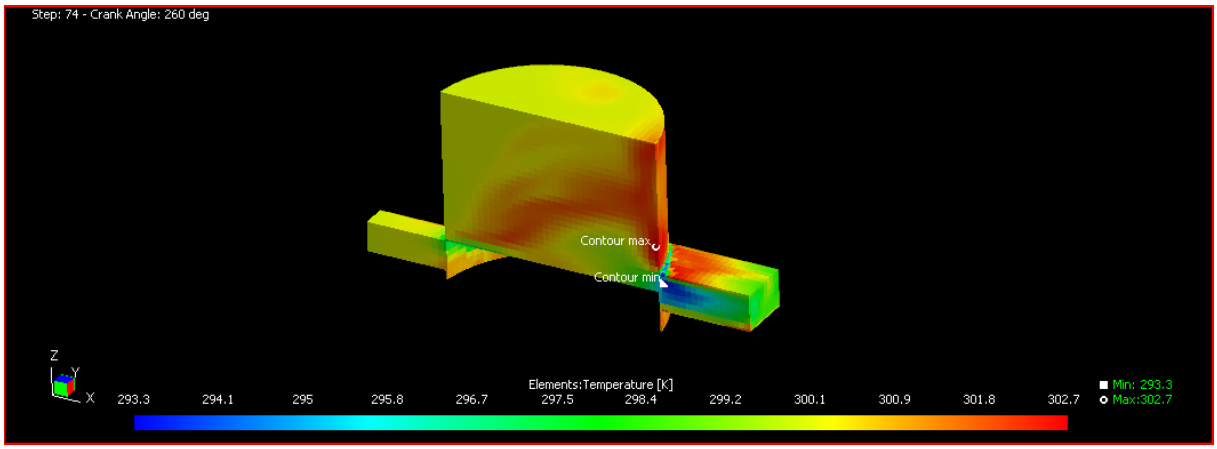

Fig. 8.10 Temperature disturbance when the intake ports closing

In Fig. 8.10, max. temperature occurs in cylinder at this crank angle. Same with the Fig. 8.8, there is a flow at the exhaust port, so pressure and temperature decreases at this location.

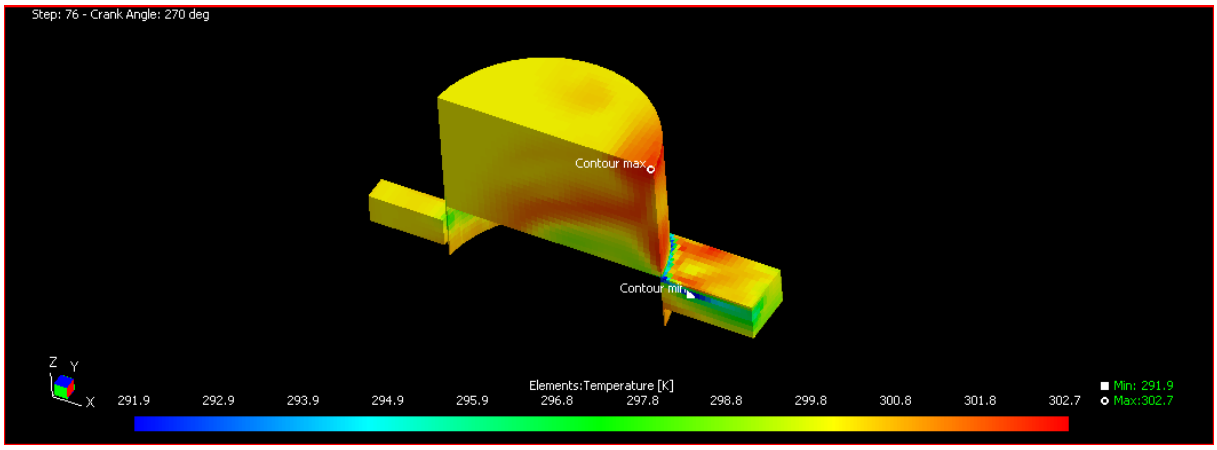

Fig. 8.11 Temperature disturbance when the exhaust port closing

In Fig. 8.11, you can see the cylinder at the 270 degrees crank angle position. At this location, max. temperature occurs in the cylinder and min. temperature occurs at the exhaust port.

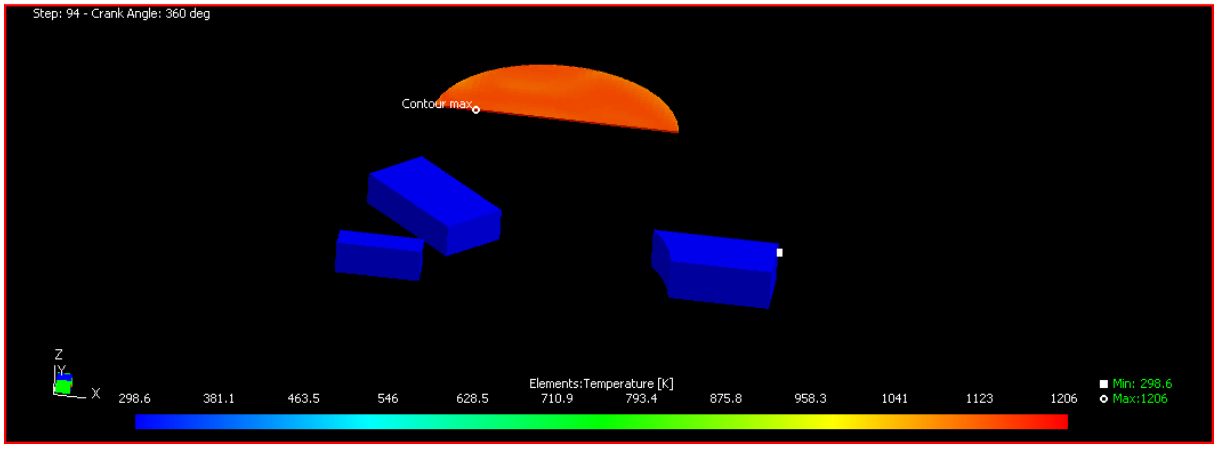

Fig. 8.12 Temperature disturbance at TDC

In Fig. 8.12, you can see cylinder at the TDC. This location, max. temperature in the all positions occurs at this crank angle. The max. temperature for this engine is 1206 K. At this position exhaust port's temperature is about 300 K.

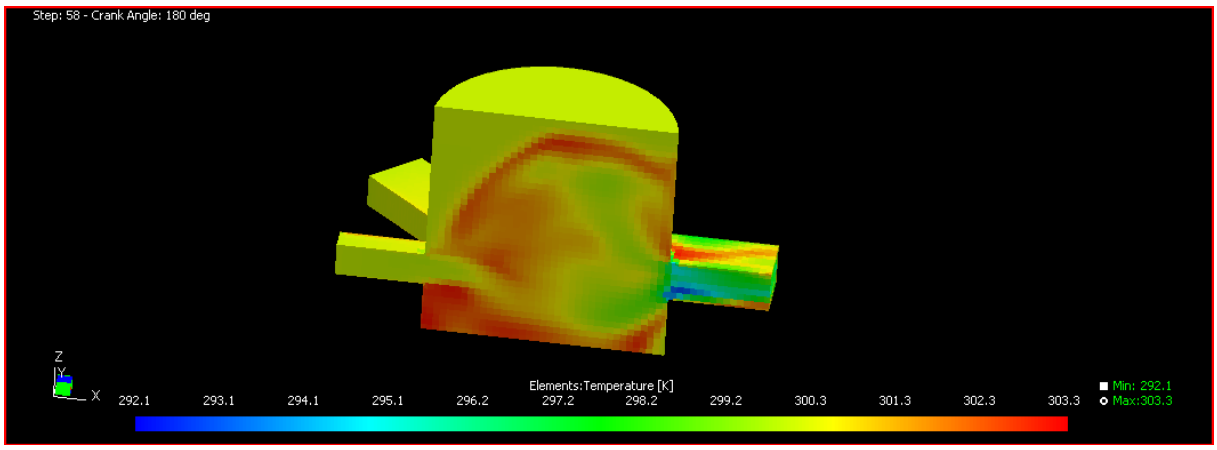

Fig. 8.13 Temperature disturbance at BDC

In Fig. 8.13, you can see the position at BDC. At this position, the coldest area is at the exhaust port again.

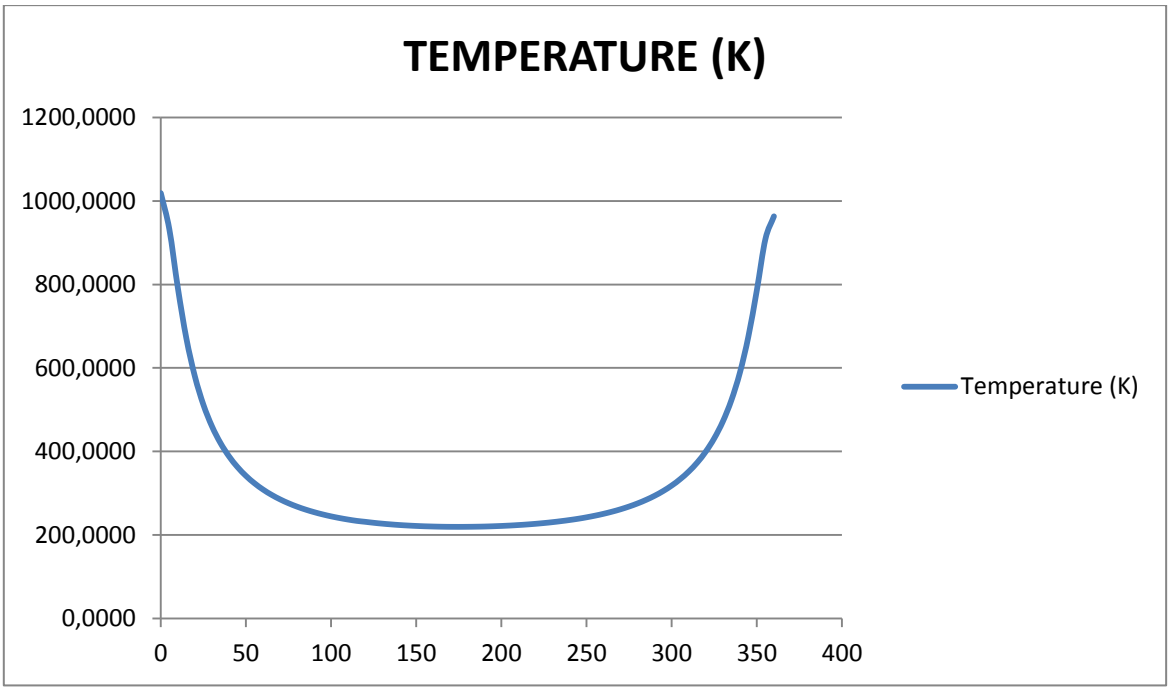

Fig. 8.14 Temperature values to crank angle

8.3 Turbulent velocity

In fluid dynamics, turbulence or turbulent flow is a flow regime characterized by chaotic property changes. This includes low momentum diffusion, high momentum convection, and rapid variation of pressure and velocity in space and time.

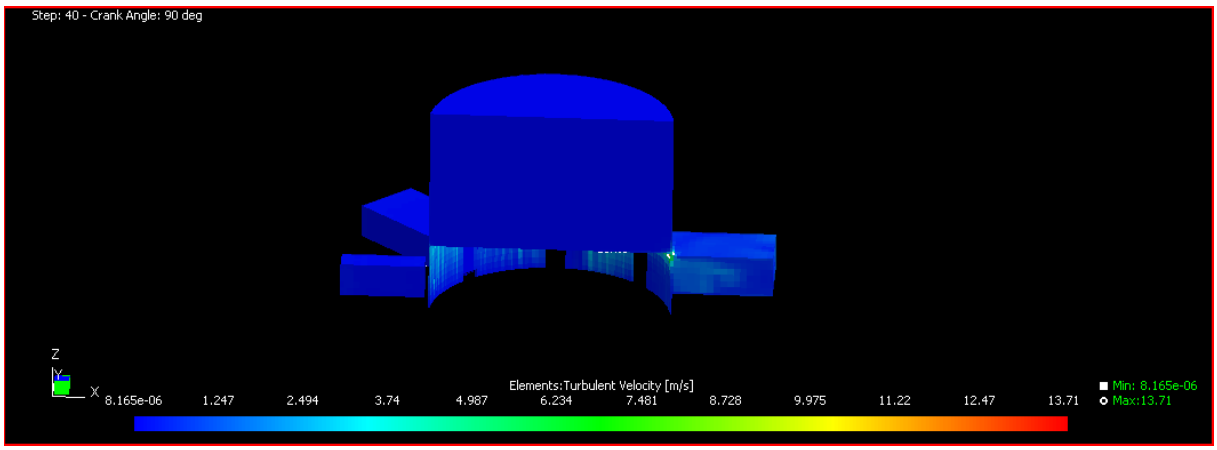

Fig. 8.15 Turbulent velocity disturbance when the exhaust port opening

In Fig. 8.15, there is no action, because all ports are closed and there is no air motion.

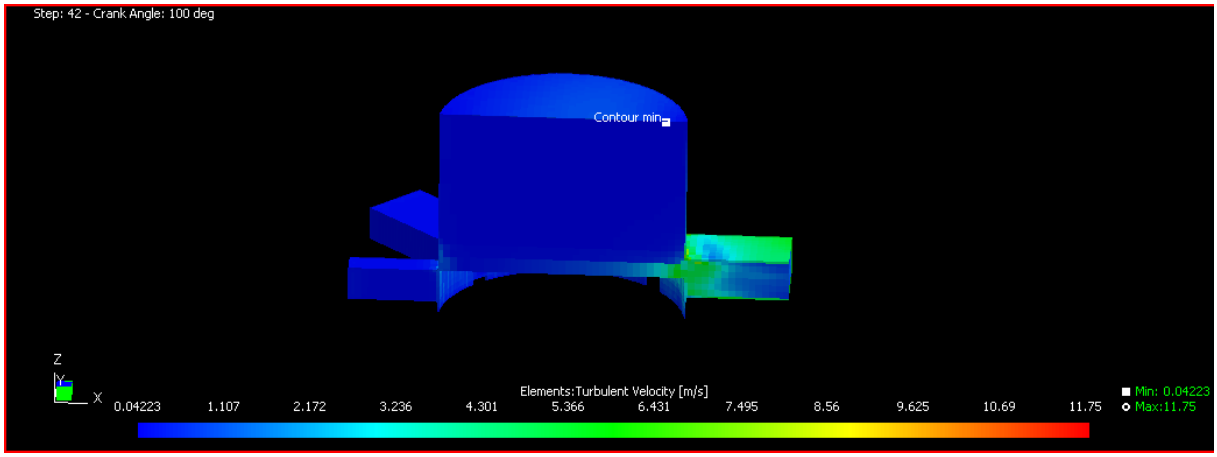

Fig. 8.16 Turbulent velocity disturbance when the intake ports opening

In Fig. 8.16, there is some action at the exhaust port. Because at this location, exhaust port is open, so air flow occurs at this location from the high pressure to the low atmosphere pressure.

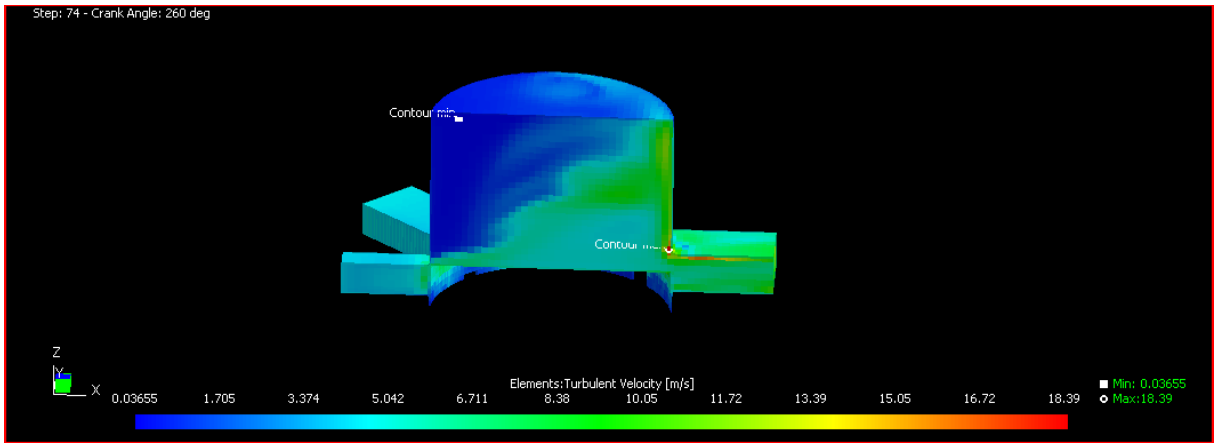

Fig. 8.17 Turbulent velocity disturbance when the intake ports closing

In Fig. 8.17, you can see the air flow from the intake ports to the cylinder. At this position, intake ports are closed. However, air motion can be seen which is take in before closing the intake ports in the cylinder. And the max. turbulent velocity occurs at the corner of exhaust port so this is because the sharp corners affect the motion of fluids.

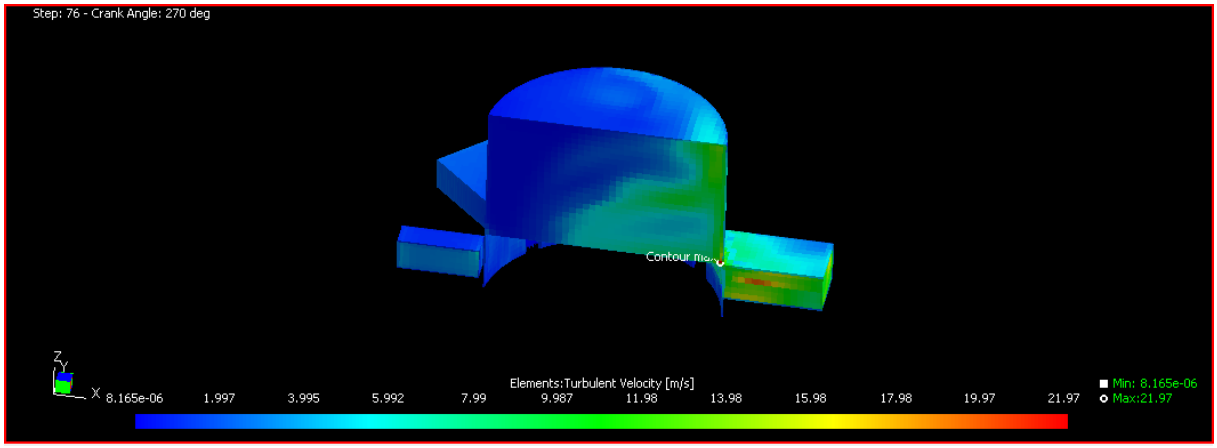

Fig. 8.18 Turbulent velocity disturbance when the exhaust port closing

In Fig. 8.18, intake ports have already closed, so there is no action. At the exhaust port, the air flow through to the atmospheric pressure can be seen. At the corner, the max. turbulent velocity occurs as Fig. 8.15.

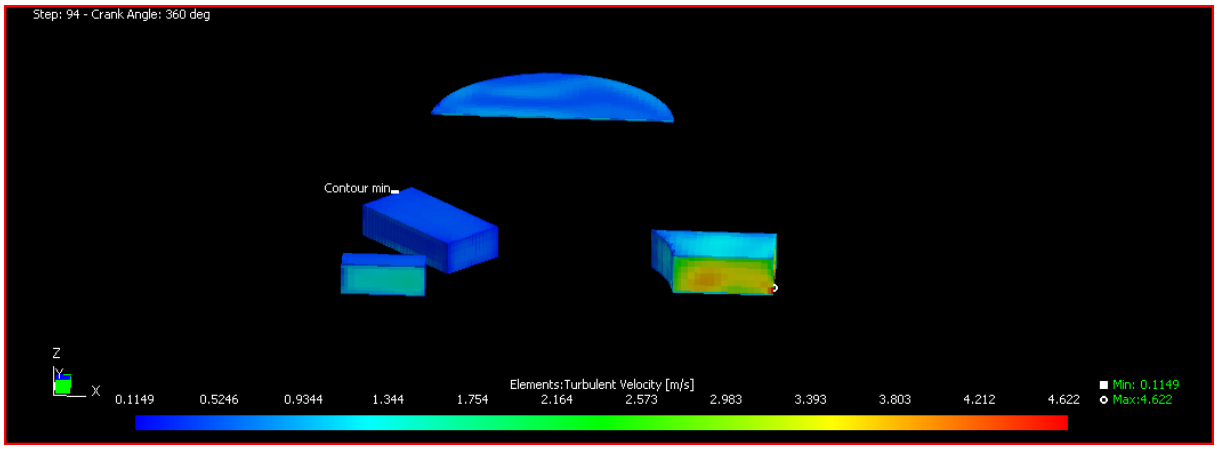

Fig. 8.19 Turbulent velocity disturbance at TDC

In Fig. 8.19, you can see cylinder at TDC and at this crank angle, max. turbulent velocity occurs at the exhaust port.

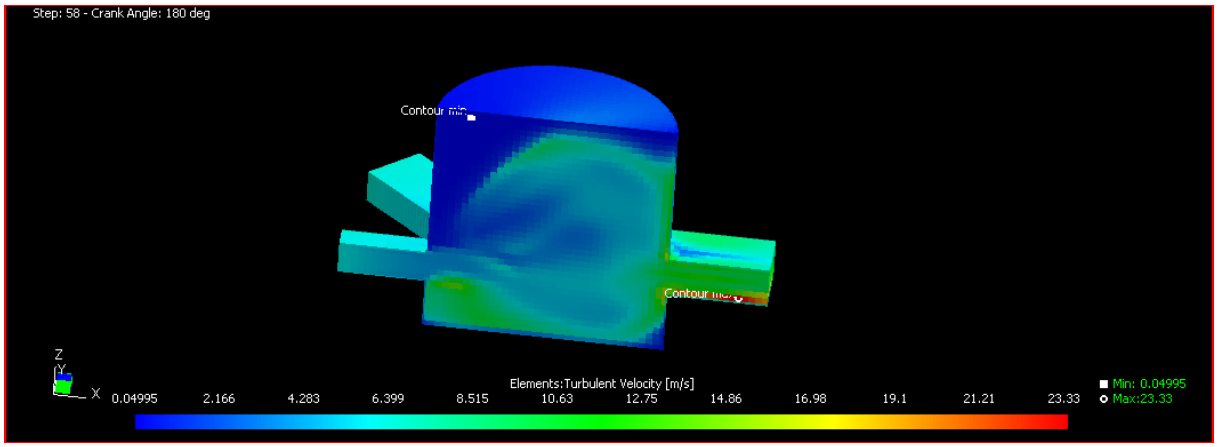

Fig. 8.20 Turbulent velocity disturbance at BDC

In Fig. 8.20, piston is at BDC. At this location, turbulent velocity reaches about the maximum point. Because, intake and exhaust ports both are open. For this reason, turbulent velocity is effective at the ports and cylinder. You can see the flow actually at the Fig. 8.18. There is a flow through the cylinder from the intake ports and thorough outside from the cylinder and exhaust port. And max. turbulent velocity occurs at the exhaust port. In addition to this, at the upper corner of the cylinder, there is no action. This is the disadvantages of this system, because this is hard to control air flow in cylinder actually. For this reason, unburned mixture can go out from the exhaust port, and this affects the engine efficiency.

9 Conclusion

The main aim of this project is can find out the conditions in cylinder to make cold flow modelling of a two-stroke engine. Analyses are made on computer with using 3-Dimensional software which is accepted on worldwide. On this project, the initial conditions are 105 kPa and 300 K.

In accordance with the informations that are signified on the upper passages, cold flow modeling of two-stroke engine has been made. The top disadvantage of two-stroke engine is much scavenging can be seen in this model. This is caused by the simple valve design of two-stroke engine. As a part of the software, Navier Stokes equations are solved numerically and a clear view of flow structure can be seen.

The project which is realized is a base for the subsequent studies. After the cold flow modeling of two-stroke engine, more efficient flow structure can be achieved to make geometrical optimizations. In this context, much scavenging can be reduced. On the next steps of this project, less emission and more efficiency can be built up to make combustion modeling with fuel with using the advantages of geometrical optimizations. In addition to this, the fuel optimization can be made in combustion modeling.

In conclusion, the amount of carbon that is given to the atmosphere can be reduced with a well-designed flow structure. Accordingly, decreasing of the rate of greenhouse effect can be provided. In addition to this, the fuel costs can be reduced to make fuel efficiency.

10 References

[1] Panagiotis Kontoulis, Christos Chryssakis and Lambros Kaiktsis, Evaluation of Pitot Injections in a Large Two-Stroke Marine Diesel Engine, Using CFD and T-φ Mapping.

[2] Yoshio Kobayashi, Yukiteru Yoshida, Kazuyuki Uenoyama, Kazunori Kudo and Hiroyuki Endo, Low Exhaust Emissions System for Small Two-Stroke Cycle Engines. Mitsubishi Heavy Industries, ltd. technical Review Vol.38 No.3 (Oct. 2001).

[3] S. Scott Goldborough and Peter Van Blarigan, Optimizing the Scavenging System for a Two Stroke Cycle, Free Piston Engine For High Efficiency and Low Emissions: A Comptational Approach. SAE technical paper series 2003-01-0001.

[4] J.Galindo, H. Cliement, B. Plá, V. D. Jiménez, Correlations for Wiebe Function Parameters for Combustion Simulation in Two-Stroke Small Engines. Applied Thermal Engineering 31 (2011) 1190-1199

[5] Hoywood, J. B. and E. Sher, 1999. The Two-Stroke Cycle Engine Its Development, Operation and Design. Taylor and Francis, UK., pp:451.

[6] Jante, A., 1968. Scavenging and other problems of two-stroke cycle sparkingnition engines. Soc. Automat. Eng. Trans., 77:1804-1824.

[7] Sher, E., 1985. A new practical model for the scavenging process in a 2-stroke cycle engine. SAE Trans., 94: 1485-1495.

[8] Reddy, K. V., V. Ganesan and K. V. Gopaklakrishnan, 1986. Under the roof of the cylinder head experimental study of the air movement in a two-stroke engine. Soc. Automat. Eng. Trans., 95: 1984-1919.

[9] Ikeda, Y., M. Hikosaka and T. Nakajima, 1991a. Scavenging flow measurements in a motored two-stroke engine by fiber LDV. Soc. Automat. Eng. Trans., 100: 990-998

[10] Hilbert, H. S. And R. E. Falco, 1991. Measurements of flows during scavenging in a Two-stroke engine. SAE Trans., 100: 999-1013.

[11] Hoywood, J. B. and E. Sher, 1999. The Two-Stroke Cycle Engine Its Development, Operation and Design. Taylor and Francis, UK., pp:451.

[12] Amsden, A.A., T.D. Butler, P.J. O'Rourke and J.D. Ramshaw, 1985. KIVA-A comprehensive model for 2-D and 3-D engine simulations, Soc. Automot. Eng. Trans., 94: 4.1-4.15.

[13] Changyou, C. and F. J. Wallace, 1987. A generalised isobaric and isochronic thermodynamic scavenging model. Soc. Automat. Eng. Trans., 96: 933-947.

[14] Raghunatha, B. D. And R. G. Kenny, 1997. CFD simulation and validation of flow within a motored teo-stroke engine. Soc. Automat. Engineers Paper 970359

[15] Ikeda, Y., M. Hikosaka, T. Nakajima and T. Ohhira, 1991b. Scavenging flow measurements in a fired two-stroke engine by fiber LDV. Soc. Automat. Eng. Trans., 100: 981-998.

[16] Yang, S. L., Y. K. Siow, C. Y: teo and K. Hanjalic, 2005. A KIVA code with Reynolds-stree model for engine flow simulation. Energy, 30: 427-445.

[17] Basha, S. A. and K.R. Gopal, 2009. In-cylinder fluid flow, turbulence and spray models: A review, Renewable Sustainable Energy Rev., 13:1620-1627.

[18] Verhelst, S. And C. G. W. Sheppard, 2009. Multi-zone modeling of spark-ingition engine combustion: An overview. Energy Conser. Manage., 50: 1326-1335.

[19] Yang, S. L., Y. K. Siow, C. Y: teo and K. Hanjalic, 2005. A KIVA code with Reynolds-stree model for engine flow simulation. Energy, 30: 427-445.

[20]] R.Mikalsen, A. P. Roskilly, A Computational Study of Free-Piston Diesel Engine Combustion.Applied Energy Volume 86, Issues 7-8, July-August 2009, pp. 1136-1143.

[21] Shyam Menon and Christopher P. Cadou, Miniaturization Limits of Small IC Engines. PowerMEMS 2009, Washington DC, USA, December 1-4, 2009.

[22] H. Ma, K. Kar, R. Stone, R. Raine and H. Thorwarth, Analysis of Combustion in a Small Homogeneous Charge Compression Assisted Ignition Engine. Int. J. Engine Res. Vol. 7 2006.

[23] http://en.wikipedia.org/wiki/Two-stroke_engine

[24] Blair Gordon, Design and Simulation of a Two Stroke Engine. 1-5.

[25] Blair Gordon, Design and Simulation of a Two Stroke Engine. 6-8.

[26] Blair Gordon, Design and Simulation of a Two Stroke Engine. 6.

[27] Blair Gordon, Design and Simulation of a Two Stroke Engine. 26-27.

[28] Blair Gordon, Design and Simulation of a Two Stroke Engine. 28.

[29] Blair Gordon, Design and Simulation of a Two Stroke Engine. 29.

[30] Blair Gordon, Design and Simulation of a Two Stroke Engine. 29-30.

[31] Blair Gordon, Design and Simulation of a Two Stroke Engine. 30-31.

[32] Blair Gordon, Design and Simulation of a Two Stroke Engine. 31.

[33] Blair Gordon, Design and Simulation of a Two Stroke Engine. 31-33.

[34] Blair Gordon, Design and Simulation of a Two Stroke Engine. 34.

[35] Blair Gordon, Design and Simulation of a Two Stroke Engine. 34-35.

[36] Frank M. White, Fluid Mechanics. 353-354.

[37] Frank M. White, Fluid Mechanics. 354-356.

[38] Frank M. White, Fluid Mechanics. 356-358.

[39] Frank M. White, Fluid Mechanics. 358.

[40]http://www.itcmp.pwr.wroc.pl/~znmp/dydaktyka/fundam_FM/Lecture_no3_Turbulent_flow_Modelling.pdf

[41]http://cfd.mace.manchester.ac.uk/twiki/pub/Main/TimCraftNotes_All_Access/fl3-navier-stokes.pdf

[42] http://www.ricardo.com/en-GB/What-we-do/Software/Products/VECTIS/

[43] http://www.ricardo.com/en-GB/What-we-do/Software/Products/VECTIS/In-cylinder-Analysis/